IMPROVEMENTS TO A BI-DIRECTIONAL FLYBACK DC-DC CONVERTER FOR BATTERY SYSTEM OF THE DC HOUSE PROJECT

A Thesis

presented to the

Faculty of California Polytechnic State University,

San Luis Obispo

In Partial Fulfillment

of the Requirements for the Degree

Master of Science in Electrical Engineering

by

Michael Wu

June 2014

COMMITTEE MEMBERSHIP

TITLE:	Improvements to a Bi-directional Flyback DC-DC Converter for Battery System of the DC House Project
AUTHOR:	Michael Wu
DATE SUBMITTED:	June 2014
COMMITTEE CHAIR:	Dr. Taufik, Professor, Electrical Engineering Department
COMMITTEE MEMBER:	Dr. Ahmad Nafisi, Professor, Electrical Engineering Department
COMMITTEE MEMBER:	Dr. Dale Dolan, Assistant Professor, Electrical Engineering Department

ABSTRACT

Improvements to a Bi-directional Flyback DC-DC Converter for Battery System of the DC House Project

Michael Wu

The DC House project relies primarily on renewable energy sources to provide DC power to the various loads of the house. However, not all renewable sources are capable of providing power at all times of the day. A back-up energy source in the form of a battery storage system must be available to meet the electrical needs of the house. A bi-directional flyback power converter was initially designed to allow a battery to charge from as well as discharge to the 48V bus line of the DC House. The design provided a 35W prototype to demonstrate the converter's feasibility. Further improvements to increase power output through changes in design as well as improving the control scheme of the bi-directional converter were conducted. Results allowed an increase of output power to 48W with efficiency at 82% for both charging and discharging. The improvements to the control scheme allowed for better management of charging and discharging cycles of the battery.

ACKNOWLEDGMENTS

I would first like to thank my family who has sacrificed so much of their time, energy and money to see me get to where I am today. They have always encouraged me to succeed in my education and have effortlessly supported me in my pursuit for a Bachelor's and Master's Degree in Electrical Engineering. Without their example and support, I would not have been able to push myself hard enough to achieve my goals.

Next I would like to thank my advisor Dr. Taufik who has inspired me throughout my university career. He has always expected the best from me whether in lecture or lab, and has sparked my desire to learn all I can about power electronics. His guidance and words of encouragement have not only challenged and helped me throughout this thesis, but will continue to do so for years to come.

I would also like to thank my colleagues and college friends who have made the past few years an experience I will never forget. I want to thank Liang Li, Kyle Chan, Janine Sato, and Gloria Chen who have given me many fun college memories, Owen Jong and Austin Luan who have provided advice and technical support during my thesis, and especially Michelle Lee who has been supportive and encouraging through my times of stress and has kept me motivated to finish what I started.

TABLE OF CONTENTS

LIST OF TABLES

LIST OF FIGURES

Chapter 1 – Introduction

1.1 Growing Energy Consumption

In a recent study by the U.S. Energy Information Administration (EIA), the world's energy consumption is estimated to increase by 56% between the years of 2010 and 2040 [1]. Figure 1-1 elaborates on this estimated growth in consumption with the projected trends for various fuel types. Renewable energy and nuclear power are each growing at 2.5% per year, but even with this thriving development, the world's energy consumption will still deeply rely on fossil fuels in the year 2040.

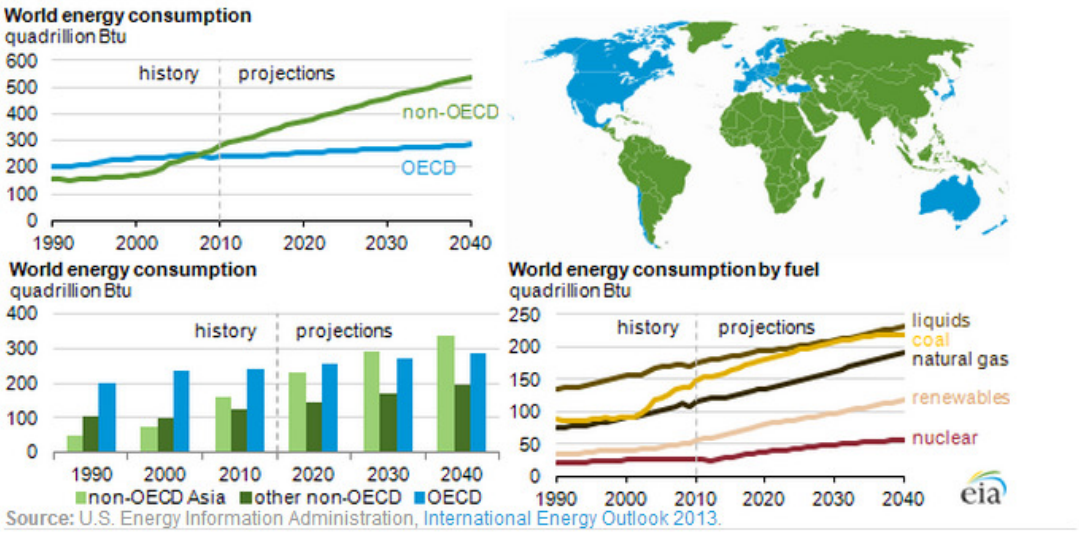

Figure 1-1: Projected World Energy Consumption from 1990 to 2040 [2]

Delivered energy sources like electricity will also follow the projections of the EIA through 2040. However, the world's total energy demand will be heavily supplied by electricity. The EIA projects a 2.2% increase per year in the world electricity delivered to end users as seen in Figure 1-2.

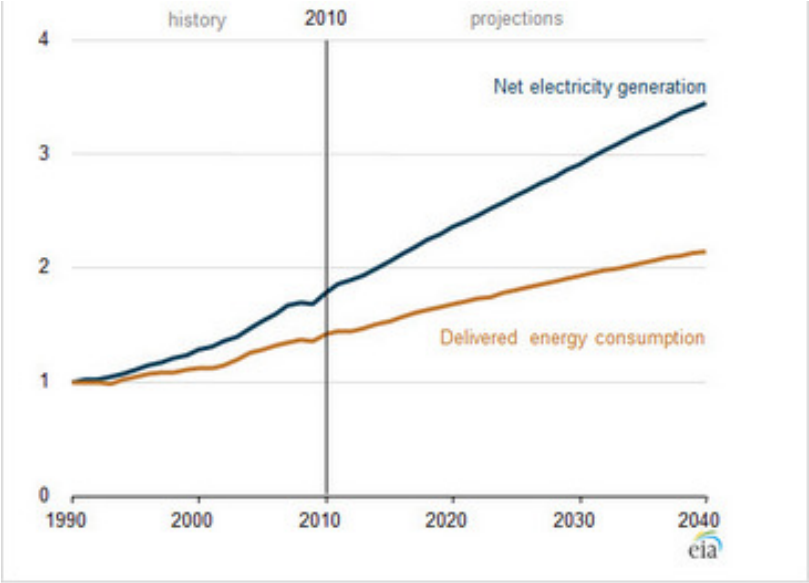

Figure 1-2: Growth of Electricity Generation and Total Energy Consumption [3]

Within the category of electricity generation, the fastest-growing sources have come from renewable energy sources, with an annual increase of 2.8% from 2010 to 2040 [3]. However, even with the progression of technology and new forms of electrical energy generation, the International Energy Agency (IEA) estimated in 2009 that about 20% of the world's population is still without access to electricity. Many of these people live in either developing Asia or sub-Saharan Africa, and in rural areas. These places, especially rural areas, are often too far away or too dispersed to be serviced by the traditional large-scale power plants. Efforts for rural electrification in such areas aim to provide energy services through methods like renewable energy, to meet demands and further human well-being and economic development.

1.2 The DC House Project

The DC House is a project started at California Polytechnic State University with the goal of providing an affordable and more efficient solution to the energy problems in developing and rural areas. The electricity being generated and transmitted from power plants are in the form of alternating current (AC). Many renewable sources generate their power through direct current (DC), meaning that before this power can be used by the consumer, it must first be converted to AC and then back into DC with the help of electronics [4]. However, this conversion introduces power loss which reduces the system's overall efficiency as well as extra costs from the necessary electronics and equipment to employ this system. The DC House aims to avoid these potential downfalls by solely relying on DC power to provide enough energy for household essentials. By removing the need to convert energy from DC to AC, power loss is minimized as well as the cost to implement the system. The DC House can be optimized to the various sources of renewable energy available in these rural areas such as solar, wind, hydro, and human power.

The DC House project is comprised of four phases. Phase 1 was completed in June of 2011, and provided the initial studies for a DC house electrical system design, generator systems, and the main multiple-input-single-output (MISO) DC-DC converter. Generator systems for the DC House consisted of photovoltaic, wind, hydro, and bicycle-powered. Phase 2, which was completed in June 2012, focused on creating a temporary DC House model as well as development in essential electrical components like a DC light bulb, 12V Wall outlet, and cell phone charger. Phase 3 concluded in June of 2013, and provided improvements to the initial designs of the MISO converter, a new battery

storage system, and additional forms of human-powered generators like a Merry-Go-Round and swing, and the distribution panel design of the house.

The DC House project is currently undergoing Phase 4 with goals of further improving distribution panel, the battery storage system, and the human-powered and hydro-electric generators. This phase also hopes to integrate all the projects from Phases 1 to 4 to provide a fully functional DC House. In 2015, this project plans to have several demonstration sites built in Indonesia to showcase the potential these DC Houses have for rural electrification. Figure 1-2 provides a top level diagram of the DC House and how the electrical energy is supplied to household appliances.

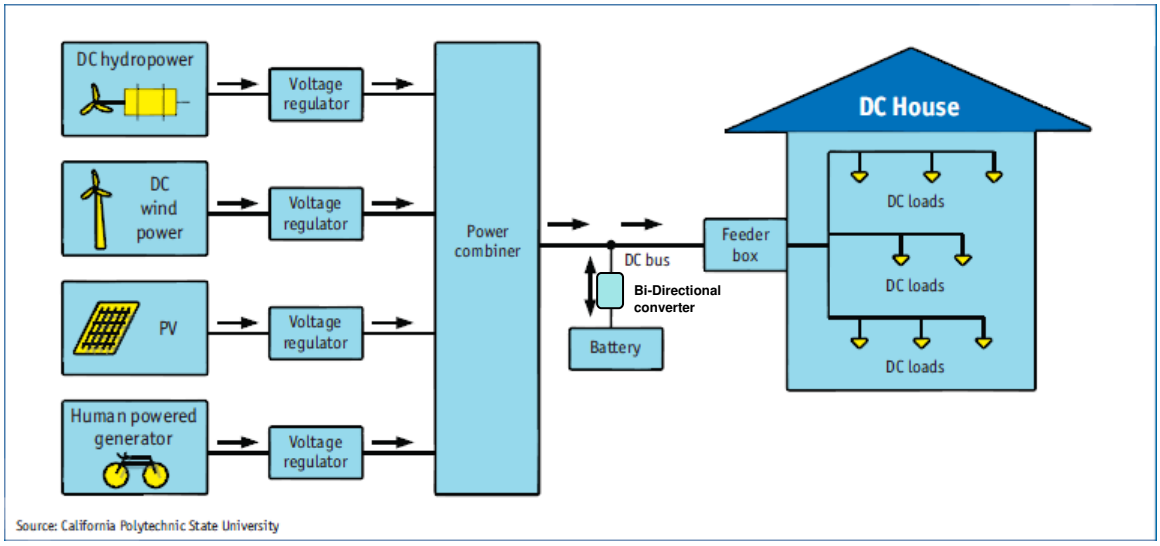

Figure 1-3: DC House System [5]

Chapter 2 – Background

2.1 Lead – Acid Batteries

The oldest type of rechargeable battery is the lead-acid battery. Despite having a very low energy-to-weight ratio and a low energy-to-volume ratio, its ability to supply high surge currents means that the cells have a relatively large power-to-weight ratio [6]. Due to these qualities as well as their cost, lead-acid batteries are widely used as storage devices in backup power supplies.

Lead-acid batteries are constructed using flat lead plates immersed in a pool of electrolyte. The batteries are made up of cells which consist of two lead plates, a positive plate covered with a paste of lead dioxide, and a negative made of sponge lead with an insulating material (separator) in between. The plates are enclosed in a plastic battery case and then submerged in an electrolyte consisting of water and sulfuric acid. Each cell is capable of storing 2.1 volts [7]. Figure 2-1 illustrates what a typical battery cell looks like.

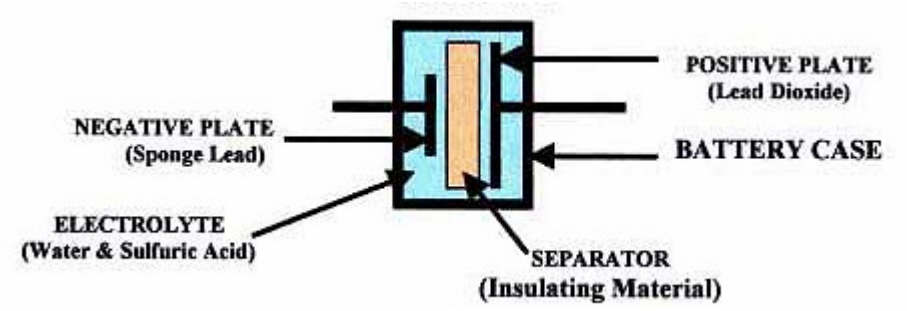

Figure 2-1: Typical Internal Configuration of a Lead-acid Battery [7]

There are two types of lead-acid batteries: starting batteries and deep cycle batteries. Starting batteries are designed to deliver quick bursts of energy and contain a

larger amount of thinner plates [8]. These batteries are typically used to start automotive engines and can be easily damaged by deep discharges. Deep cycle batteries have less instant energy, but greater long-term energy delivery. Deep cycle batteries have thicker plates and can survive a number of discharge cycles [8]. Since deep cycle batteries can be frequently discharged, they are more suitable for applications in photovoltaic systems, electric vehicles, and uninterruptible power supplies [6].

Lead-acid batteries are given an amp hour (AH) rating with a standard Amp rating taken for 20 Hours. For example a 100AH rated battery means that if you draw from the battery for 20 hours, it will provide 100 amp-hours or 5 amps per hour (5A x 20hr = 100AH) [9].

A typical 12V lead-acid battery will output 12.6V when fully charged and 10.5V when fully discharged [7]. Discharging the battery to voltages lower than 10.5V is not recommended because it can severely damage it. There are several different methods of recharging a lead-acid battery, but two typical techniques are slow and quick-charging. Each of these has their own rate of charge based on the current. Slow-charging requires a current of 2A whereas quick-charging requires 6A or 10A. Using a slow charge rate of 2A is much safer and is less harsh on the lead-acid battery allowing it to have a longer lifetime. However with slow-charging, it can take roughly 8 -10 hours to fully charge the battery compared to two hours on a quick-charge rate.

2.2 Bidirectional DC-DC Converters

Renewable energy sources like wind, solar, and hydro are often unpredictable and do not provide a constant output of power. Buildings that rely on renewable energy sources often have additional energy storage systems like batteries or super -capacitors to provide energy when the renewable source is unavailable or low. These systems greatly depend on DC-DC converters with the capability of transferring energy in two directions to provide power when sources are not present, and to replenish the storage system when it is not needed.

Basic DC-DC converters like buck and boost converters are limited to unidirectional power flow due to the diodes and the MOSFET switches in their circuitry. These circuit components only allow current to flow from input to output and are incapable of reverse current flow from output to input.

Most bidirectional DC-DC converters are characterized by a current fed or voltage fed on one side as shown in Figure 2-2**.** These converters can also be categorized into either a buck or boost type by the placement of the energy storage device. A Buck type converter has the energy storage on the high voltage side and steps down voltage from high to low. Whereas a Boost type converter has the energy storage on the low voltage side and steps up voltage from low to high.

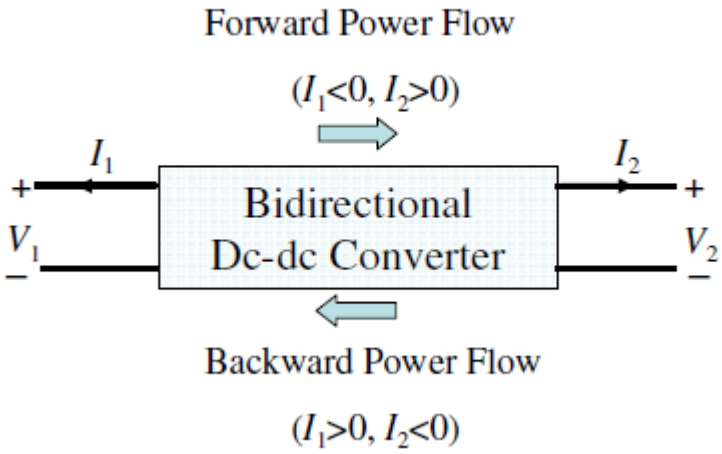

Figure 2-2: Bidirectional DC-DC Converter Characteristics [10]

As mentioned before, basic unidirectional DC-DC converters contain components that do not allow for bidirectional energy flow. By incorporating double-sided current switch cells to replace the main commutating switch and output diode, bidirectional current flow can be achieved. These cells can be implemented with a unidirectional semiconductor power switch in parallel with a diode [10] as seen in Figure 2-3. When the switch S1 is open and switch S2 is open, current can flow from left to right, but when S1 is open and S2 is closed, current is able to flow from right to left. Figure 2-4 also illustrates this design using the Boost converter.

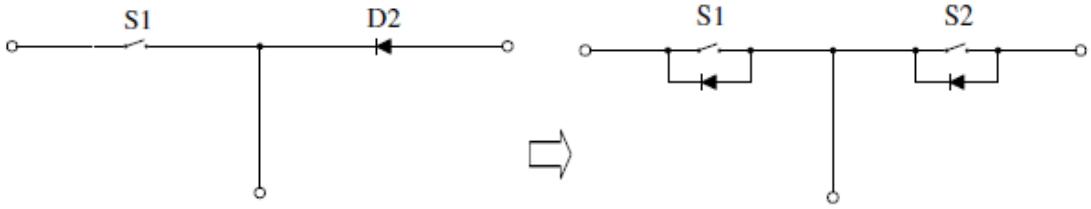

Figure 2-3: Implementation of Switch Cells in Bidirectional Converter [10]

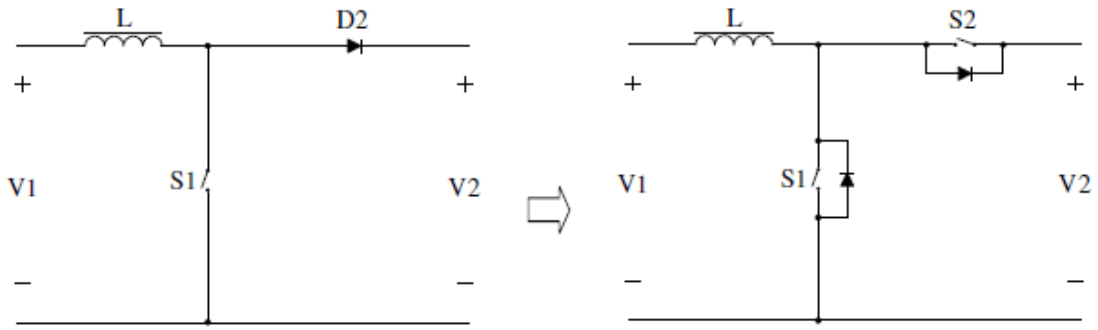

Figure 2-4: Implementation of Switch Cell in a Boost Topology [10]

All bi-directional converters can be separated into two categories: non-isolated and isolated. The commonly used non-isolated converters are buck, boost, and buck-boost where inductors are used as the primary form of energy storage. During each switching cycle of the converter, the inductor is charged by the source during the switch's on-time. The energy stored in the inductor is then discharged to the load for the remaining duration of the switching cycle. Because these converters use inductors instead of transformers like the ones in isolated converters, non-isolated topologies have advantages in terms of efficiency, size, weight, and cost. However, converters like the buck-boost cannot provide wide voltage-conversion ranges because of the equivalent series resistance (ESR) of the inductors and capacitors [11]. Isolated topologies such as flyback, forward, half-bridge, and full-bridge are advantageous in terms of safety, simplicity in control, and noise reduction. The use of transformers for energy storage also makes these topologies fit for high power and high voltage applications as desired voltage levels can be achieved by adjusting the turns-ratio of the transformers. However, these circuits are often more complex than non-isolated, and require snubbers to alleviate the high voltage stress on the MOSFET switches.

2.3 Current Bidirectional Design

The current bi-directional converter design as presented in [12] for the DC House project incorporates the flyback topology. The flyback was chosen because it yields low costs, good transient response, requires a low amount of components, and the use of the transformer to compensate for low duty cycle [12]. The availability of commercial flyback controllers on the market also makes this topology a reasonable choice as the basis for a bi-directional converter. This converter is used for the battery system that will act as a backup for the 48V bus provided by a multiple input single output (MISO) converter powered by renewable energy sources. It consists of two sides, a discharging side to supply power to the house when the bus is down, and a charging side to recharge the battery system. The objective of this thesis is to further improve the initial study and design of the bi-directional converter used for the battery system. Data and results obtained from the initial study are used to make appropriate changes and improvements to design a converter that can supply the desired power output for the DC House. A new control strategy will also be implemented to better regulate the charging and discharging of the lead-acid batteries in hopes to prolong their life. Lastly, a physical demonstration of the completed system will be conducted as part of Phase 4 of the DC House project. Results from the simulation and hardware implementation of the improved converter will be documented in this report along with lessons learned and suggestions to further improve the design.

Chapter 3 – Design Requirements

3.1 Battery Configuration

In the initial design of the bi-directional converter and battery system done in 2013, a single lead-acid car battery was chosen as the storage device. Series or parallel-connected batteries were considered for their ability to increase overall voltage or amp-hour rating respectively, however this battery system needed to be designed for locations where resources were not readily available. The battery set-up will remain a single lead-acid car battery as specified in [12].

3.2 Bidirectional Converter Specifications

With the chosen storage device and the specifications of a single lead-acid battery stated in Chapter 2, the input and output voltages, and output current requirements of the bi-directional converter are determined. Because the charging side of the bi-directional converter is connected to the 12V lead-acid car battery, the converter will require a minimum of 12V output voltage to properly charge the battery. In the initial design presented in [12], a output voltage of 12.5V is chosen to compensate for any switching or leakage loss from the converter. However this does not account for the natural resistance of the battery. The rule of thumb for setting a charging voltage is 2.4V per cell [13]. For a 12V battery, the level should be set at a minimum of 14V and a maximum of 14.5V, with 14.4V as the desired target [13]. Therefore, the output voltage of the charging side of the bi-directional converter will be 14.4V. The output current of the charging side will depend on charging rate that is specified in Chapter 2. For safety reasons and concerns of the longevity of the batteries, a slow-charging current of 2A will be used. The input voltage of the charging stage will come from the established 48V bus line of the DC

House. This bus line is directly connected between the front-end generation and the DC House feeder [12]. The bi-directional converter will be connected in between generation and the DC House, therefore the input voltage of the charging stage will be 48V. With the specified output voltage and current, the output power of the charging side of the bi-directional converter will be 29W.

As stated in Chapter 2, a typical 12V lead-acid battery will output 12.6V when fully charged and 10.5V when fully discharged. These two voltages will be used as the maximum and minimum input voltages respectively for the discharging side of the bi-directional converter. From the initial designs of the bi-directional converter, the output power of the discharging stage was calculated and chosen on a "worst-case" scenario of 10 hours of discharging from the lead-acid battery. Table 3-1 shows the time it takes for the lead-acid battery to be depleted at certain power outputs and DC House load currents with an output voltage of 48V to the bus line. A power output of 300W with a maximum output current of 6.25A was chosen which has a discharge time of 15.36 and 11.20 hours with respects to their amp rating [12]. This maximum power output will allow the battery to pass the “worst-case” scenario of 10 hours to fully discharge the battery. The output voltage of the discharging stage will be 48V as the system is designed to supply the established bus line voltage when power is needed and generation is unavailable.

Table 3-1: Preliminary Values of Discharging Time Based Upon Output Power and Lead-Acid Battery Amp Rating [12]

		For 96AH	For 70AH
Output Power (W)	**Current From DC House Load (A)**	**Time to Discharge (Hours)**	**Time to Discharge (Hours)**
500	10.42	9.22	6.72
450	9.38	10.24	7.47
400	8.33	11.52	8.40
350	7.29	13.17	9.60
300	6.25	15.36	11.20
250	5.21	18.43	13.44
200	4.17	23.04	16.80
150	3.13	30.72	22.40
100	2.08	46.08	33.60

3.3 Control System Requirements Overview

Lead-acid batteries are very sensitive to both deep discharge and overcharging. Repeated deep discharges and overcharging can easily destroy the battery so it becomes a necessity to protect them by controlling the charging and discharging processes [14]. In a stand-alone photovoltaic (PV) system, charge controllers are commonly used to provide this type of regulation. Their primary function is to protect the battery from overcharge and over-discharge [15]. Basic charge controllers operate using set points. Two important set points are the Voltage Regulation Set Point (VR), and the Low Voltage Disconnect (LVD). The VR is the maximum voltage that a controller allows the battery to reach. At this point a controller will either discontinue battery charging or begin to

regulate the amount of current delivered to the battery. The LVD is the voltage at which the load is disconnected from the battery to prevent over-discharge [15].

Two basic methods exist for controlling or regulating the charging of a battery in a PV system which are series and shunt regulation. A shunt controller regulates the charging of a battery by interrupting the PV current by short-circuiting the array. A blocking diode is required in series between the battery and the switching element to keep the battery from being shorted [15]. A series controller regulates the charging of a battery by using series-interrupting where battery charging is terminated when voltage reaches a VR set point.

The current control scheme of the bi-directional converter is a series controller that uses a LT1716 comparator to control which stage the converter operates in. A LVD set point is placed at 11V disconnecting the load when voltage drops below this point. The controller will also activate the charging stage when the battery's terminal voltage drops below 11V. As stated in Chapter 2, a new control strategy that better regulates the charging and discharging of the lead-acid battery is required. This new control scheme should incorporate both VR and LVD set points to prevent overcharge and over discharge.

3.4 Bidirectional Converter Design Requirements Overview

In order to prolong the lifetime of the lead-acid car battery, the efficiency of the bi-directional converter becomes an important consideration. Continuing with the initial design using separate flyback topologies, the bi-directional converter is expected to have efficiency greater than 80% at maximum load for both the charging and discharging

converters. The output voltage ripples of both the charging and discharging stages are expected to be less than 5% of their respective output voltages of 14.4V and 48V. Line and load regulations will be less than 5% as well for both stages.

The initial design of the discharging stage for the bi-directional converter had an output power of 48W. However 48W will not be sufficient to power all the devices of the DC House. As proposed earlier an output power of 300W at 6.25A will be considered for the improved design. The charging converter of the bi-directional converter will have an output power of 25W with a slow charging current of 2A. Table 3-2 summarizes the design requirements of the proposed bi-directional converter.

Table 3-2: Specifications of the Bi-Directional DC-DC Converter

	Charging Stage	**Discharging Stage**
Input Voltage	48V ±5%	(11-13V), 12V Nominal
Output Voltage	14.4V	48V
Maximum Output Current	2A	6.25A
Maximum Output Wattage	29W	300W
Line Regulation	5%	5%
Load Regulation	5%	5%
Output Voltage Ripple	5%	5%
Efficiency at Full Load	≥80%	≥80%

Chapter 4 – Design and Simulation Results

In this chapter, the design of the proposed bi-directional converter from Chapter 3 will be elaborated upon. The converter will comprise of two separate flyback circuits that will charge or discharge the battery system of the DC House. The charging stage of the converter will transfer energy from the DC bus line of 48V to the terminals of the 12V lead-acid battery and the discharging stage of the converter will transfer energy from the battery to the DC bus line. This chapter also documents the calculation of component sizes to meet the design requirements. Simulation results for each stage and the bi-directional converter with a new control scheme are presented as well. A section of this chapter will also detail the design of custom flyback transformers used in the bi-directional converter.

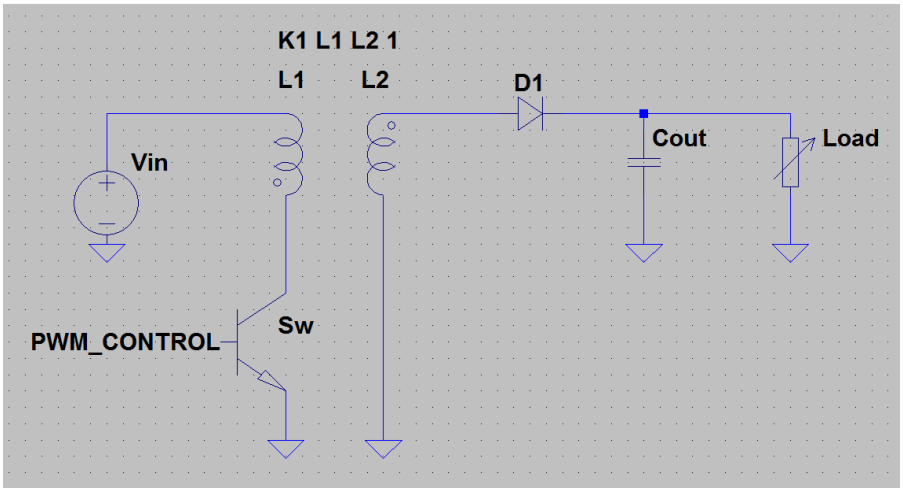

Figure 4-1: Basic Flyback Circuit Diagram

4.1 Operation of the Flyback Topology

As seen in Figure 4-1, the flyback circuit does not require many components to operate. The flyback also uses its transformer's magnetizing inductance as an energy storage device, removing the need for external inductors like in boost and buck topologies. The circuit is able to store energy through charging and discharging of the magnetizing inductance. When the switch is on, the input voltage source provides current that will flow through the primary winding of the transformer and the switch which will cause energy to be stored in the magnetizing inductance. The induced voltage on the secondary side is negative due to the dot convention of the primary and secondary windings causing the output diode to be reversed bias. The current supplied to the load comes from the output capacitor.

When the switch is off, the energy stored in the transformer is released through the secondary winding. The secondary voltage becomes positive causing the output diode to conduct and load current is supplied by the magnetizing inductance. This allows the output capacitor to recharge for the next on-cycle of the switch.

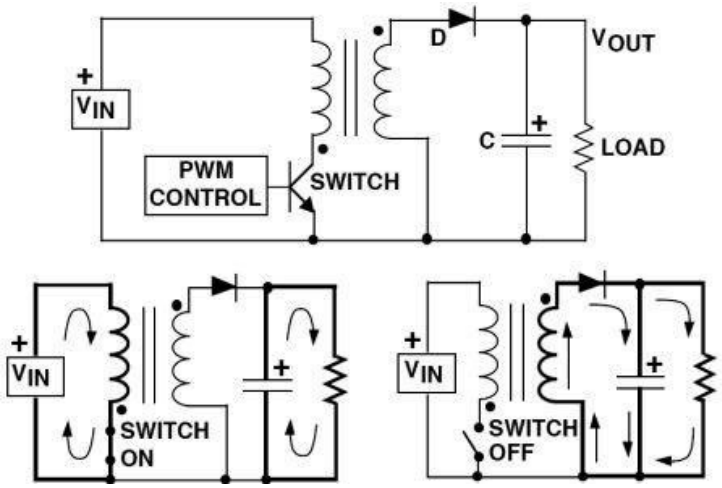

Figure 4-2: Basic Operation of Flyback Topology [16]

The flyback topology offers a wider range of controller chips that are easily accessible for commercial use compared to other topologies like buck-boost, full-bridge, and half-bridge, which are also commonly used in bi-directional converters. Taking into consideration the design specifications listed in Chapter 3, the LT3748 flyback controller from Linear Technology was chosen due to its wide input voltage range, power rating, and primary-side feedback load regulation capabilities [17]. This controller also operates in boundary condition mode which allows for output voltage to be derived from the primary side of the transformer when the secondary current is zero. This feature removes the need for an opto-coupler for feedback, reduces transformer size, and improves load regulation [17]. Figure 4-3 shows a block diagram of the LT3748 flyback controller.

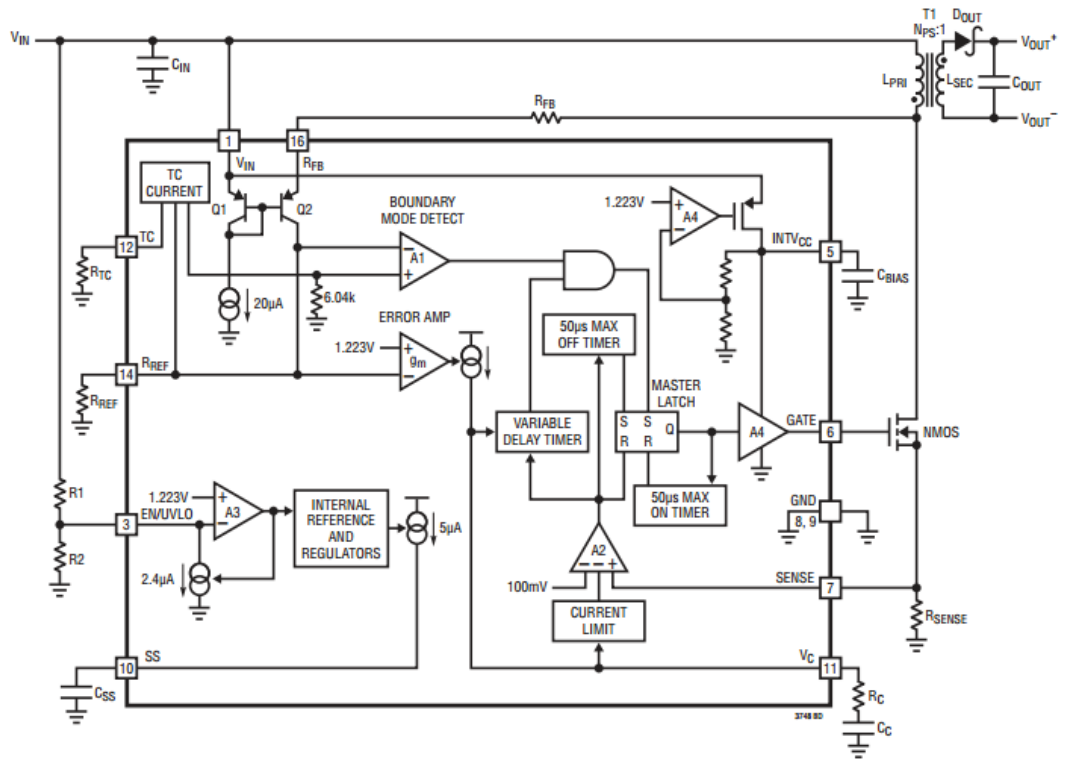

Figure 4-3: LT3748 Block Diagram [17]

4.2 Charging Stage Flyback Design

The charging stage of the bidirectional converter needed to be capable of a maximum output power of 29W as specified in Chapter 3. The power output of the LT3748 controller is limited by the external components of the IC, so sizing components correctly based on the specifications provided in the datasheet are important.

The duty cycle (D) of the controller can be determined using the following equation found in the LT3748 datasheet [17]:

$$D = \frac{(V_{out}+V_{F(diode)})*N_{PS}}{V_{in}+(V_{out}+V_{F(diode)})*N_{PS}} \quad (4.1)$$

D: Duty cycle

N_{PS}: Turns ratio of the flyback transformer $\frac{N_P}{N_s}$

$V_{F(diode)}$: Forward voltage drop across output diode in Volts

V_{in}: Input voltage of the converter in Volts

V_{out}: Average output voltage of the converter in Volts

With a chosen turns ratio of 4:1, a forward voltage drop of 1V, an input voltage of 48V, and an average output voltage of 14.4V, the duty cycle of the controller is approximately 58%.

To optimize the current limit of the primary side, the controller utilizes a sense resistor that can be calculated using the following equations [17]:

$$R_{sense} = \frac{100mV}{I_{Lmin}} \tag{4.2}$$

$$I_{Lmin} = I_{omax} * \frac{2}{N_{PS}*0.85*(1-D)} \tag{4.3}$$

R_{sense}: Sense resistance in Ω

I_{Lmin}: Minimum peak primary side inductance current in Amps

I_{omax}: Maximum average output current in Amps

Using Equation 4.3, the minimum primary side peak current is determined to be 2.51A with I_{omax} at 2A, a turns ratio of 4 and a duty cycle of 0.58. To allow for headroom, the peak current value calculated is rounded up to 3A which corresponds to a sense resistor value of 33mΩ. The sense pin of the controller is highly susceptible to noise, which can negatively affect the operation of the flyback circuit. To counter this potential issue, a

low pass filter using a 100Ω resistor and 10nF capacitor with a cutoff frequency of 160 kHz was connected to the pin before the sense resistor [12].

In order to meet the output current requirements of the charging stage, a proper transformer has to be selected. The turns ratio and minimum primary inductance of the transformer will be determined using equations found in the LT3748 datasheet. More detail about the design of the flyback transformers will be provided later in this chapter. A turns ratio of 4:1 was determined based on the input and output voltages of the converter. The input voltage of 48V is 3.4x the output voltage of 14V. Rounding up on the turns ratio allows for a more obtainable transformer. The primary inductance of the transformer must satisfy the three requirements prescribed in the datasheet of the controller. This inductance value must exceed the minimum values determined by the following equations [17]:

$$L_{PRI} \geq \frac{(V_{out}+V_{F(diode)})*R_{sense}*N_{PS}*t_{settle(\min)}}{V_{sense(\min)}} \tag{4.4}$$

$$L_{PRI} \geq \frac{V_{in(\max)}*R_{sense}*t_{on(\min)}}{V_{sense(\min)}} \tag{4.5}$$

L_{PRI}: Primary Inductance in Henrys

$t_{settle(min)}$: Minimum settling time in seconds

$t_{on(min)}$: Minimum on-time of GATE pin in seconds

The sampling circuitry needs a minimum of 400ns to settle and sample the output voltage while the MOSFET switch is off, and the LT3748 has internal circuit constraints that prevent it from setting the GATE node high for shorter than approximately 250ns [17].

With the previously mentioned parameter values, a minimum sense voltage of 15mV, and a maximum input voltage of 50V, Equations 4.4 and 4.5 provide the minimum values for the primary inductance which are calculated to be 60.17µH and 28µH respectively. The maximum primary inductance value for the transformer is constrained by the full-load operating frequency $f_{sw(min)}$ [17]. This maximum value is determined by the following equation [3748DS]:

$$L_{PRI} \leq \frac{V_{in(\min)} * N_{PS} * (V_{out} + V_{F(diode)})}{f_{sw(\min)} * I_{Lmin} * (N_{PS} * (V_{out} + V_{F(diode)}) + V_{in(\min)})} \tag{4.6}$$

$f_{sw(min)}$: Minimum switching frequency in Hz

$V_{in(min)}$: Minimum input voltage in Volts

Assuming a minimum input voltage of 45V, and a minimum switching frequency of 42kHz, the maximum primary inductance value is calculated to be 216.23µH. This means that the primary inductance must fall between the range of 60.17µH and 216.23µH. The primary inductance of the flyback transformer is chosen to be 168µH which will give a secondary inductance of 10.5µH with a turns ratio of 4:1.

The switching MOSFET and output diode of the flyback are sized based on the two equations provided in the datasheet [17].

$$V_{DS(\max)} = V_{in(\max)} + V_{out(\max)} * N_{PS} \tag{4.7}$$

$$V_{RRM} = V_{out(\max)} + \frac{V_{in(\max)}}{N_{PS}} \tag{4.8}$$

$V_{DS(max)}$: Maximum drain-source voltage in Volts

V_{RRM}: Maximum diode reverse voltage in Volts

Equations 4.7 and 4.8 provide a minimum value for component sizes of the switching MOSFET and output diode. Assuming a maximum input voltage of 50V, a maximum output voltage of 14V, and a turns ratio of 4, the maximum drain-source voltage is 113.6V and the maximum diode reverse voltage is 25.17V. The chosen MOSFET will need to have a rated value higher than 113.6V and a low $R_{DS(on)}$ resistance to improve efficiency. Taking this into consideration, a Fairchild FDS2582 MOSFET rated at $150V_{DS}$ with a continuous drain current of 4.1A was chosen. As for the output diode, it will need a rated value at or higher than the calculated value with low forward diode voltage drop. The Fairchild MBRS340 rated at 40V will be used. For simulation purposes, a Vishay Si4490DY MOSFET and MBRB2545CT Schottky will be used as substitutes for the chosen components.

To meet the output voltage ripple specification, a large enough output capacitor is required. Using the specifications from Chapter 3, the minimum output capacitance can be calculated from the following equation [18]:

$$C_{min} = \frac{D}{R_{min} * f_{min} * \frac{\Delta V}{V_{out}}} \tag{4.9}$$

C_{min}: Minimum output capacitance in Farads

Assuming duty cycle (D) is 58%, a minimum switching frequency of 42kHz, a minimum load resistance of 7Ω, output voltage of 14V and a peak-to-peak ripple voltage of 5%, the minimum output capacitance needed is 39.8µF. A 100µF capacitor rated at 16V will be chosen as the output capacitor.

To regulate the output voltage, the LT3748 used a resistor ratio between the feedback resistor in the primary side and a reference resistor [17]. The reference resistor can range from 5.76kΩ to 6.34kΩ, but is suggested to be set at 6.04kΩ. The feedback resistor value is obtained through the following equation provided by the datasheet [17]:

$$R_{FB} = \frac{V_{out}}{V_{BG}} * N_{PS} * R_{REF} \tag{4.10}$$

R_{FB}: Feedback resistance in Ω

V_{BG}: Bandgap voltage in Volts

R_{REF}: Reference resistance in Ω

Assuming the bandgap voltage is 1.223V, the reference resistor set at 6.04kΩ, a turns ratio of 4, and an output voltage of 14.4V, the feedback resistor R_{FB} is calculated to be 312kΩ.

The LT3748 also has an enable/undervoltage lockout feature that will shut-off the controller. A resistive divider is implemented between the input voltage and the EN/UVLO pin of the controller which will create a voltage that is compared to the threshold voltage of 1.223V. If the reference voltage drops below this threshold the controller will shut-off. To calculate the resistors for the voltage divider, the following equation found in the datasheet is provided [17]:

$$1.223V = 48V * \frac{R_2}{R_1 + R_2} \tag{4.11}$$

The resistive values for R1 and R2 were calculated to be 412kΩ and 15.4kΩ respectively.

The loop-gain compensation for the LT3748 is important to the transient performance and stability of the converter. The controller uses an external resistor-capacitor network for compensation and suggests using R_c =50kΩ and C_c=1nF [17]. The R_c value affects the transient performance of the circuit. If too small of a value is chosen, the circuit's transient performance suffers, but if too large of a resistor is chosen, then it will be susceptible to high frequency noise. The value of C_c affects the stability and transient performance of the circuit. Too small of a capacitance will make the circuit unstable, but too high of a capacitance will hurt transients. Taking these consequences into account, R_c and C_c are chosen to be 10kΩ and 4.7nF respectively.

The internal circuitry of the controller is powered by the voltage at the $INTV_{cc}$ pin. Looking at the suggested configurations for the LT3748, a 4.7µF capacitor will be connected in series with the $INTV_{cc}$ pin and ground.

Figure 4-4 shows the 48V to 14V flyback converter with the calculated component values denoted above. The soft-start and temperature compensation pins will be configured based on recommendations in the datasheet since they are features of the controller that will not be used for the charging circuit of the bidirectional converter.

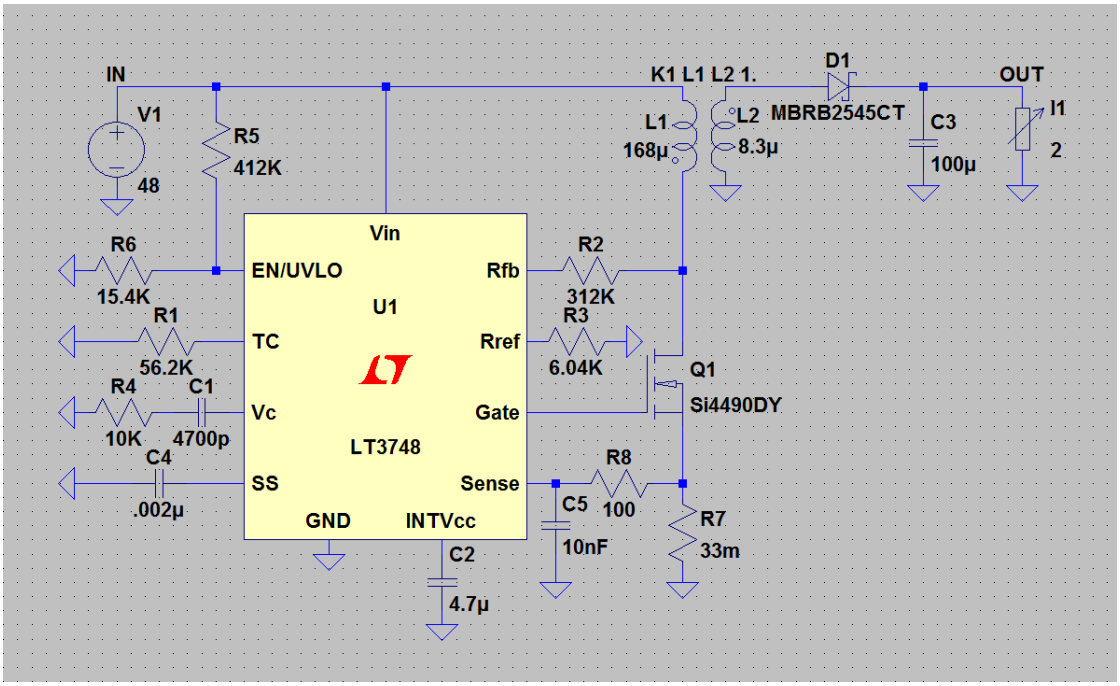

Figure 4-4: 48V to 12V Charging Flyback

4.3 Charging Stage Flyback Simulation Results

Table 4-1 lists the simulation results for the charging flyback. Data on output voltage, current, power and efficiency are taken for load currents of 0.5A to 2A. Figure 4-5 shows the output voltage ripple at full load of 2A with nominal input voltage of 48V. The peak-to-peak ripple is determined to be 183.275mV or 1.31% of the output voltage. The converter's average output voltage at full load is 14.375V. Figure 4-6 shows the simulation voltage seen at the sense pin of the controller. Since the voltage on the sense pin drops to zero, the chip is running in boundary conduction mode like it should be.

Table 4-1: Simulation Data for Charging Flyback

I_{in} (A)	I_{out} (A)	V_{in} (V)	V_{out} (V)	P_{in} (W)	P_{out} (W)	Eff %
0.64	2	48	14.375	30.578	28.751	94.03
0.48	1.5	48	14.397	22.985	21.599	93.97
0.33	1	48	14.415	15.588	14.41	92.44
0.17	0.5	48	14.441	8.1391	7.2238	88.75
0.61	2	50.4	14.378	30.817	28.747	93.28
0.66	2	45.6	17.375	30.212	28.766	95.21

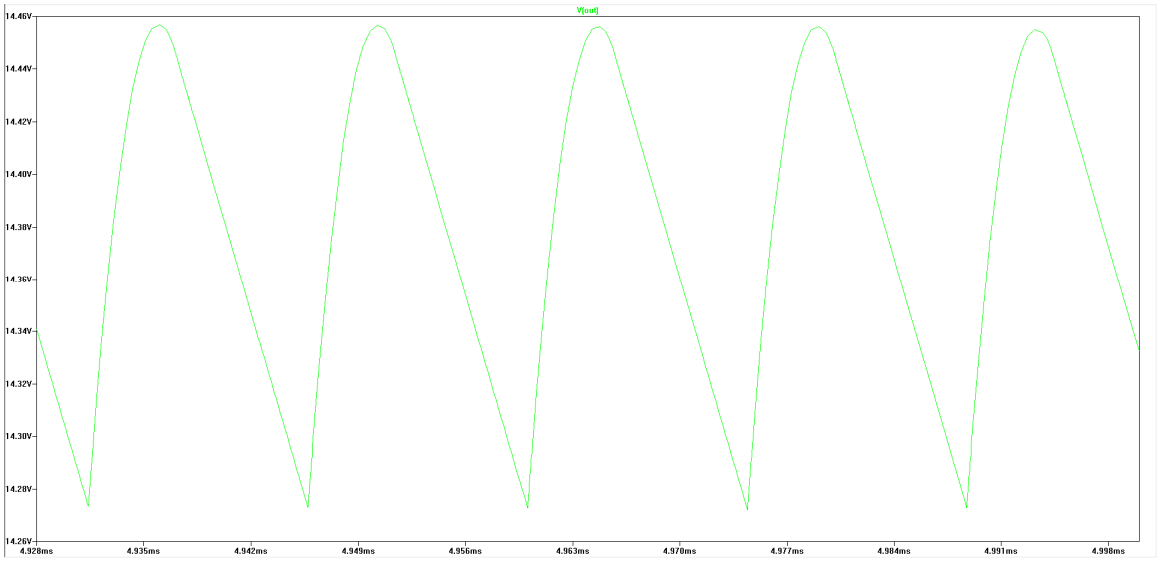

Figure 4-5: Simulated Output Voltage Ripple at Full Load (2A) of Charging Flyback

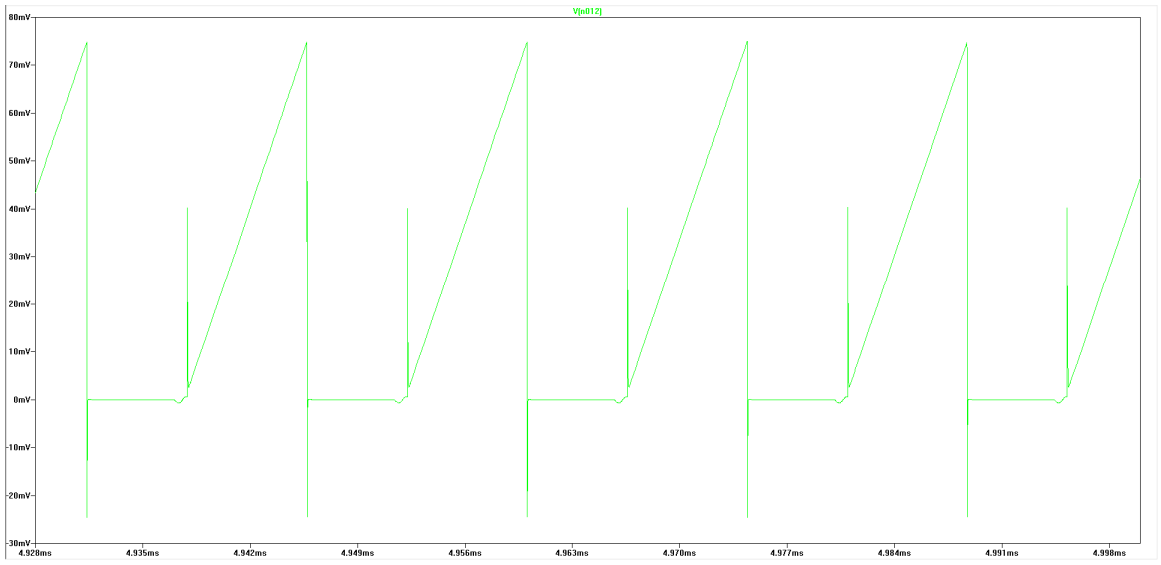

Figure 4-6: Simulated Sense Pin Voltage at Full Load (2A) of Charging Flyback

With the data from Table 4-1, line and load regulation can be calculated using the following equations:

$$Line\ Regulation = \frac{V_{out(hi-input)} - V_{out(lo-input)}}{V_{out(nom-input)}} * 100\% \quad (4.12)$$

$$Load\ Regulation = \frac{V_{out(min-load)} - V_{out(max-load)}}{V_{out(max-load)}} * 100\% \quad (4.13)$$

The line regulation is determined to be 0.021% and the load regulation is 0.459%. Figure 4-7 shows the efficiency of the converter ranging from minimum load current at 0.5A to maximum load current at 2A. The simulation results for the charging flyback meet the design specifications of Chapter 3.

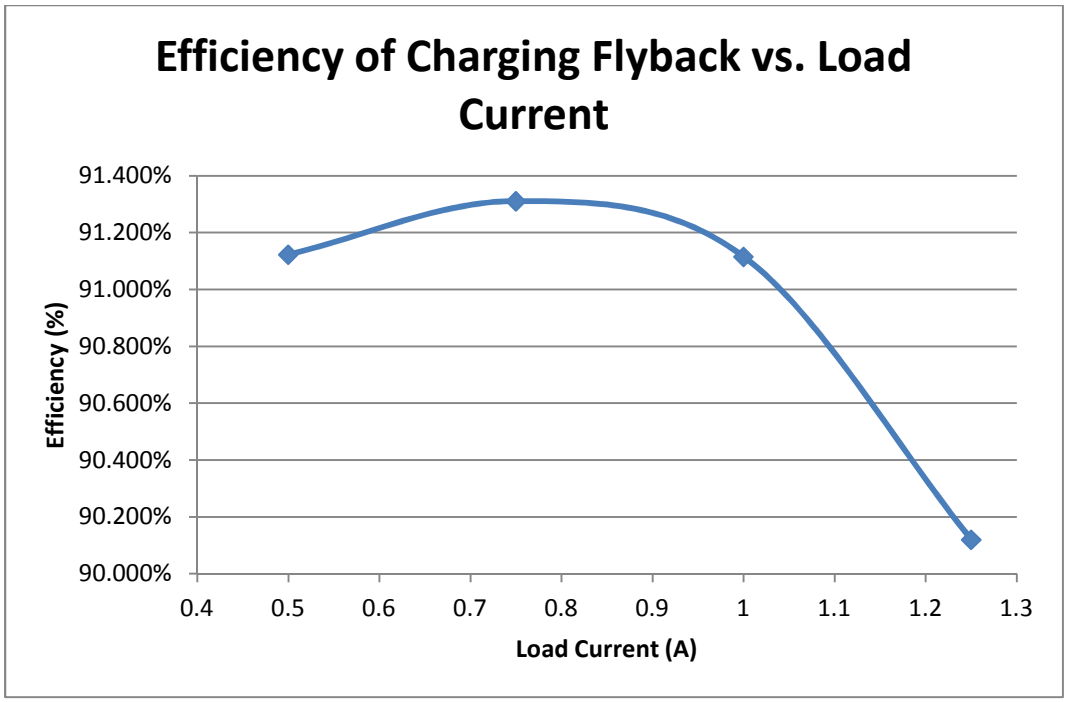

Figure 4-7: Efficiency of Charging Flyback with Varying Load Current

4.4 Discharging Stage Flyback Design

The design of the discharging stage of the bidirectional converter follows much of the same procedures as the charging stage. The first design presented in [12] was aiming to achieve an output power of 60W, but was only able to produce 34W. The improved design will produce the original goal of 60W at 1.25A full load current utilizing the LT3748 controller. The first design of this discharging flyback used a turns ratio of 1:4 at a duty cycle of 51% to boost input voltage from 12V to 48V. However, with the advantages of the flyback topology, it is possible to adjust both turns ratio and duty cycle to obtain a desired output voltage. The transfer function for a basic flyback is as follows [19]:

$$V_{out} = V_{in} * N * D \tag{4.14}$$

Where N is the turns ratio and D is the duty cycle. For an improved design, a smaller turns ratio of 1:2 will be chosen to increase duty cycle and allow for better power transfer to the output.

The duty cycle of the discharging flyback with a turns ratio of 1:2 can be determined using the following equation:

$$D = \frac{(V_{out}+V_{F(diode)})*N_{PS}}{V_{in}+(V_{out}+V_{F(diode)})*N_{PS}} \quad (4.1)$$

Assuming a 1V forward voltage drop, input voltage at 12V and an output voltage of 48V, the new duty cycle is approximately 89%.

Using Equation 4.2 and 4.3, minimum peak inductance current and sense resistor for the discharging stage is determined to be 13.5A and 7mΩ respectively. The maximum output current will be 1.25A with a duty cycle of 0.89. This converter will incorporate the same low pass filter as the charging stage to counter high frequency noise.

$$R_{sense} = \frac{100mV}{I_{Lmin}} \quad (4.2)$$

$$I_{Lmin} = I_{omax} * \frac{2}{N_{PS}*0.85*(1-D)} \quad (4.3)$$

As with the charging stage, the minimum and maximum primary inductance values for the discharging flyback transformer are determined using Equations 4.4, 4.5, and 4.6.

$$L_{PRI} \geq \frac{(V_{out}+V_{F(diode)})*R_{sense}*N_{PS}*t_{settle(\min)}}{V_{sense(\min)}} \quad (4.4)$$

$$L_{PRI} \geq \frac{V_{in(\max)} * R_{sense} * t_{on(\min)}}{V_{sense(\min)}} \tag{4.5}$$

$$L_{PRI} \leq \frac{V_{in(\min)} * N_{PS} * (V_{out} + V_{F(diode)})}{f_{sw(\min)} * I_{Lmin} * (N_{PS} * (V_{out} + V_{F(diode)}) + V_{in(\min)})} \tag{4.6}$$

The minimum on-time and minimum settling time remain at 250ns and 400ns respectively. The maximum input voltage of converter will be 13V, and the minimum input voltage will be 11.4V. The output voltage is 48V with a turns ratio of 0.5. The range for the primary inductance becomes $2.61\mu H \leq L_{PRI} \leq 17.37\mu H$. A primary inductance of 4µH will be chosen which corresponds to secondary inductance of 16µH with a turns ratio of 1:2. These values will be important when the transformer design is further discussed later in this chapter.

The switching MOSFET and the output diode must be sized correctly using the following two equations:

$$V_{DS(\max)} = V_{in(\max)} + V_{out(\max)} * N_{PS} \tag{4.7}$$

$$V_{RRM} = V_{out(\max)} + \frac{V_{in(\max)}}{N_{PS}} \tag{4.8}$$

Assuming a maximum input voltage of 13V, a nominal output voltage of 48V, and a turns ratio of 0.5, the maximum drain-source voltage is 108.6V and the maximum output diode reverse voltage is 54.3V. The International Rectifier IRFS4127TRLPBF MOSFET rated at $200V_{DS}$ with a continuous drain current rating of 72A will be used as the switch. A Vishay V10P10-M3/86A Schottky diode with a peak reverse voltage rating of 100V will be used as the output diode. For simulation purposes, a Vishay Si4490DY MOSFET and a MBR20100CT Schottky diode will substitute the chosen components.

The size of the output capacitor will dictate the output voltage ripple of the converter. Using Equation 4.9, the minimum output capacitance is determined. Assuming a duty cycle of 0.89, minimum load resistance of 38.4Ω, minimum switching frequency of 42kHz, output voltage of 48V and a 5% peak-to-peak ripple, the minimum capacitance needed for the output is 11µF.

$$C_{min} = \frac{D}{R_{min} * f_{min} * \frac{\Delta V}{V_{out}}} \tag{4.9}$$

A 30µF capacitor rated at 60V will be used as the output capacitor of the discharging stage.

The resistor ratio between the feedback resistor and reference resistors will aid the controller to regulate the output voltage to the specified level. The reference resistor can range from 5.76kΩ to 6.34kΩ, but is nominally set to 6.04kΩ. Using Equation 4.10, the feedback resistance is calculated.

$$R_{FB} = \frac{V_{out}}{V_{BG}} * N_{PS} * R_{REF} \tag{4.10}$$

Assuming the bandgap voltage is 1.223V as noted by the LT3748 datasheet, an output voltage of 48V, a turns ratio of 0.5, and a reference resistance of 6.04kΩ, the feedback resistance is 118.5kΩ.

The LT378's enable/undervoltage lockout feature shuts off the controller if input voltage drops below the minimum. A resistive divider will provide a voltage to the EN/UVLO pin that is compared to a reference voltage of 1.223V [17]. The resistance values for this divider are determined by Equation 4.15.

$$1.223V = 10.5V * \frac{R_2}{R_1+R_2} \quad (4.15)$$

A minimum input voltage of 10.5V will be used as a worst-case scenario when the lead-acid batteries are completely discharged. The resistances R_1 and R_2 are determined to be 1.4kΩ and 10kΩ respectively.

The compensation pin of LT3748 uses a resistor-capacitor network to help compensate the switching regulator. Typical values for the series RC are 50kΩ and 1nF. As mentioned before, the values of R_c and C_c have an effect on the transient performance. A 10kΩ resistor in series with a 4.7nF capacitor will be used for the series RC network.

The $INTV_{cc}$ pin provides power to the internal circuitry of the controller. A capacitor will be placed in series with the pin and ground as suggested by the datasheet. Remaining pins for temperature compensation and soft-start will be configured with recommended components provided in theLT3748 datasheet. Figure 4-8 shows the 12V to 48V charging stage flyback converter with calculated component values.

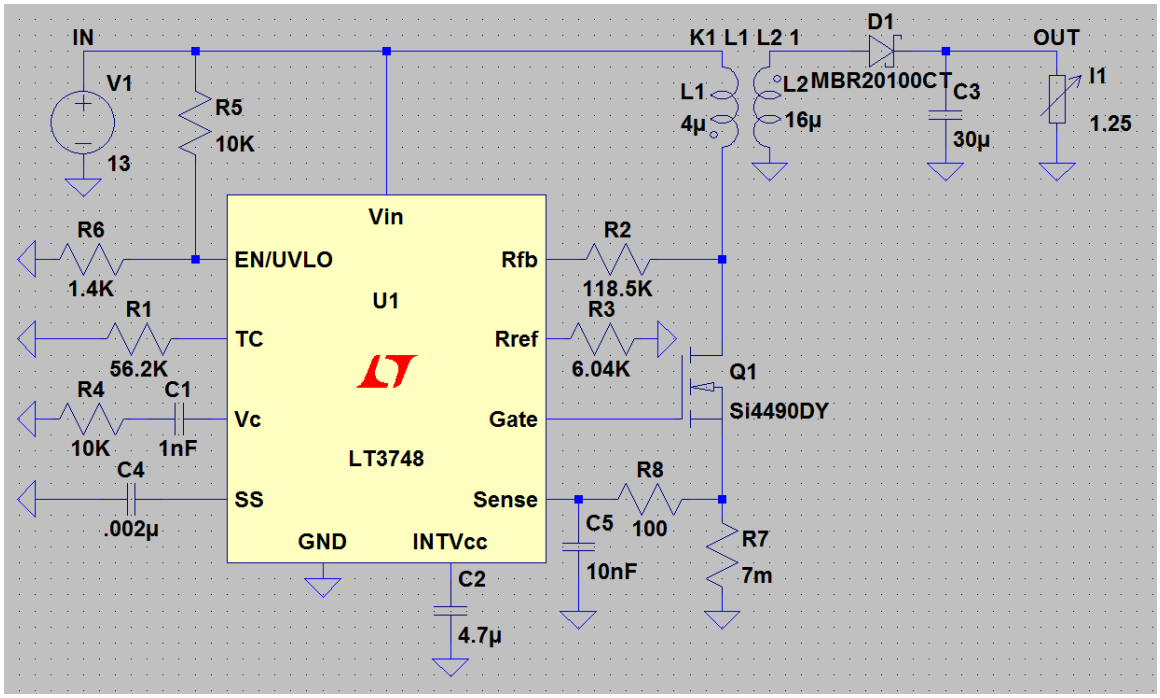

Figure 4-8: 12V to 48V Discharging Flyback

4.5 Discharging Stage Flyback Simulation Results

Table 4-2 lists the simulation results for the discharging flyback. Data on output voltage, current, power and efficiency are taken for load currents of 0.25A to 1.25A. Figure 4-9 shows the output voltage ripple at full load of 1.25A with nominal input voltage of 12V. The peak-to-peak ripple is determined to be 216.15mV or 0.45% of the output voltage. The converter's average output voltage at full load is 47.8V. Figure 4-10 shows the simulation voltage seen at the sense pin of the controller. Since the voltage on the sense pin drops to zero, the chip is running in boundary conduction mode like it should be.

Table 4-2: Simulation Data for Discharging Flyback

I_{in} (A)	I_{out} (A)	Vi_n (V)	V_{out} (V)	P_{in} (W)	P_{out} (W)	Eff %
5.49	1.25	12	47.791	65.85	59.35	90.12
4.38	1	12	47.851	52.51	47.85	91.11
3.28	0.75	12	47.931	39.36	35.94	91.31
2.20	0.5	12	48.183	26.43	24.09	91.12
1.17	0.25	12	50.127	14.09	12.53	88.90
5.98	1.25	11	47.77	65.74	59.71	90.83
5.08	1.25	13	47.8	66.1	59.75	90.39

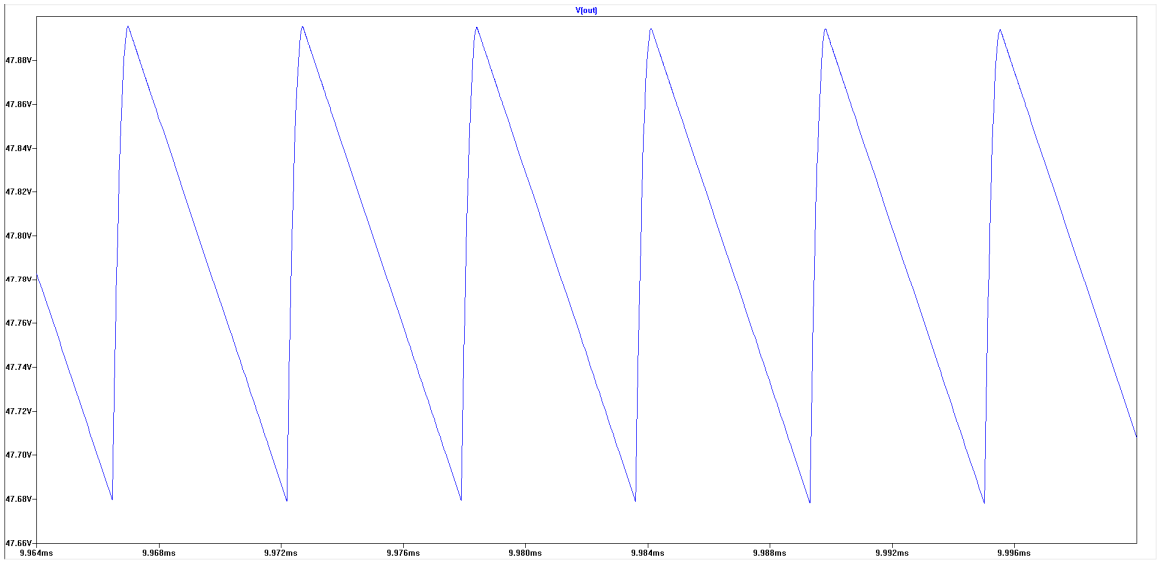

Figure 4-9: Simulated Output Voltage Ripple at Full Load (1.25A) of Discharging Flyback

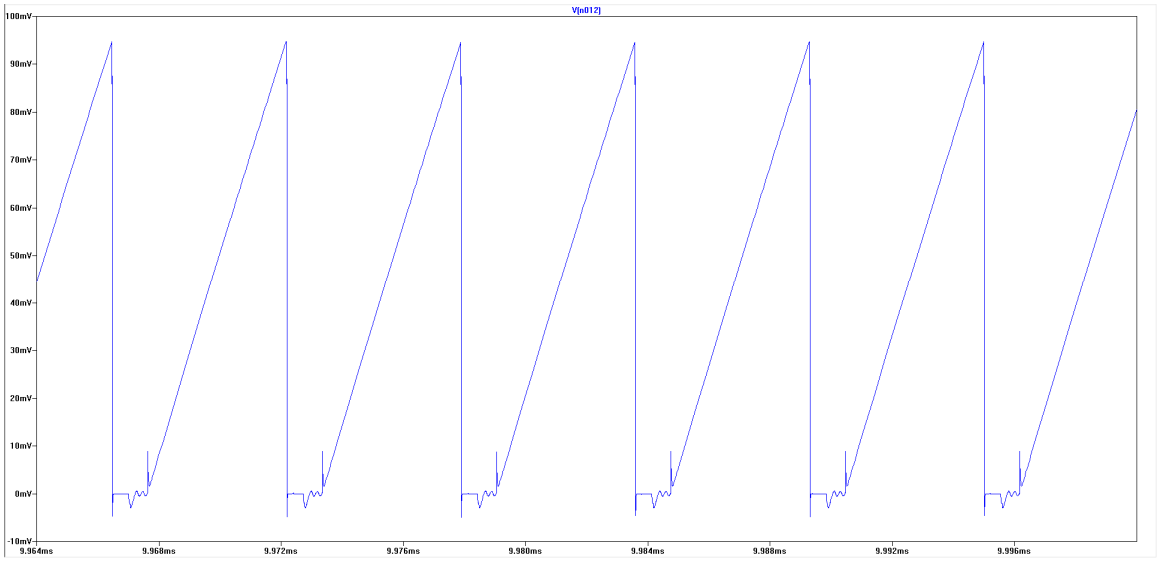

Figure 4-10: Simulated Sense Pin Voltage at Full Load (1.25A) of Discharging Flyback

With the data from Table 4-2, line and load regulation can be calculated using the same equations from the charging flyback simulation:

$$Line\ Regulation = \frac{V_{out(hi-input)} - V_{out(lo-input)}}{V_{out(nom-input)}} * 100\% \quad (4.12)$$

$$Load\ Regulation = \frac{V_{out(min-load)} - V_{out(max-load)}}{V_{out(max-load)}} * 100\% \quad (4.13)$$

The line regulation is determined to be 0.06% and the load regulation is 1.06%. Figure 4-11 shows the efficiency of the converter ranging from minimum load current at 0.25A to maximum load current at 1.25A. The simulation results for the discharging flyback meet the design specifications of Chapter 3.

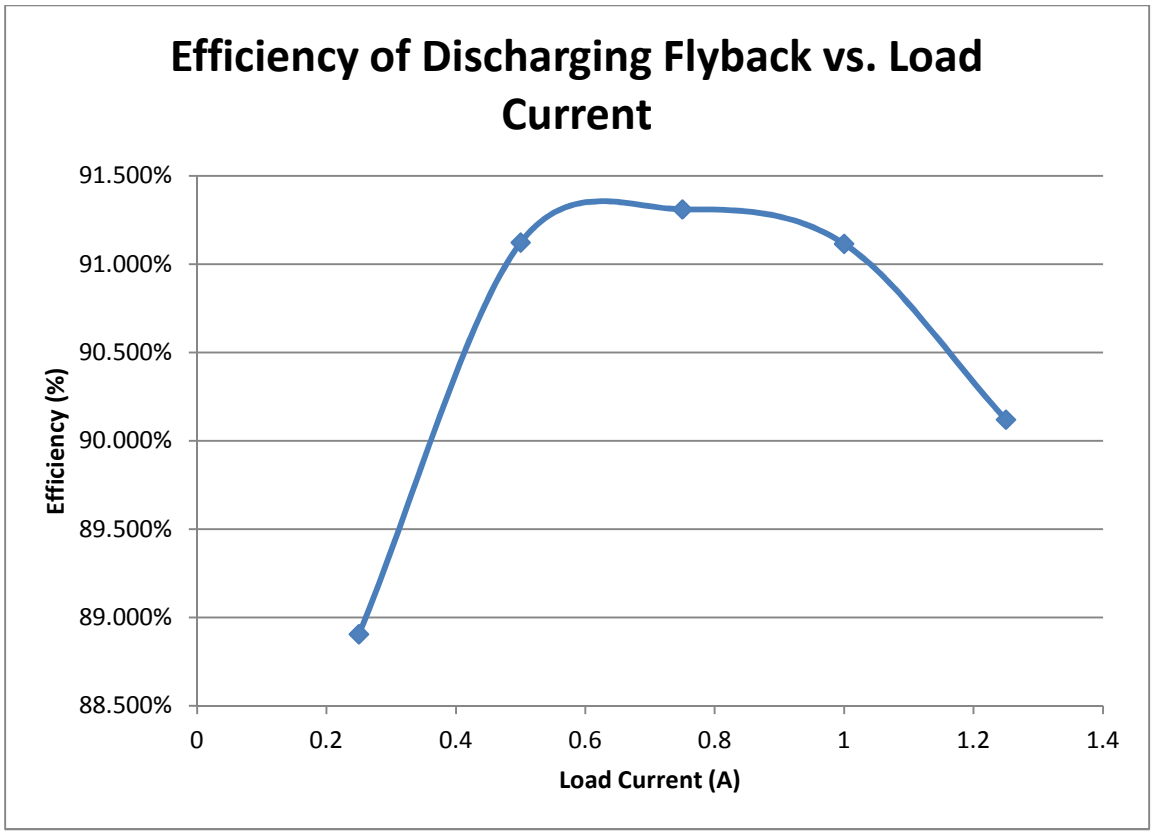

Figure 4-11: Efficiency of Discharging Flyback with Varying Load Current

4.6 Bi-directional Flyback Control Scheme Design

The control scheme of the bi-directional converter needs to be able to turn-on or off either one of the converters based on the voltage level of the battery and DC bus line. This control scheme will utilize the enable/undervoltage lockout feature of the LT3748 chips for the charging and discharging converters. Figure 4-12 shows how to configure the LT3748 to have a shutdown option by connecting a MOSFET switch in parallel to the second resistor of the resistor divider.

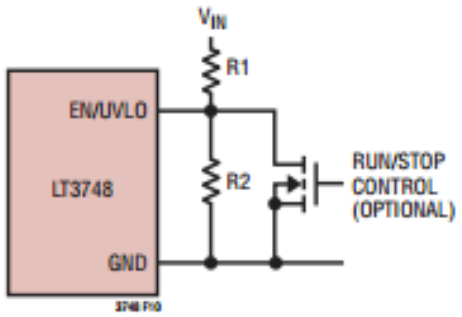

Figure 4-12: Undervoltage Lockout Shutdown Option [17]

The first design for the control scheme of the bi-directional converter utilizes the shutdown option and the voltage level of the battery. A LT1716 comparator is used to compare the lead-acid batteries voltage to a reference voltage set by the DC bus line. When the lead-acid battery voltage level is above 11V, the LT1716 will send the bias voltage as an output to shut down the discharging LT3748 controller to allow the charging LT3748 controller to turn on. When the lead-acid battery voltage level falls below 11V, the LT1716 does not send any output voltage, disabling the discharging LT3748 controller and does not provide a bias voltage for the MOSFET on the resistive network of the charging LT3748 EN/UVLO pin. This allows the charging LT3748 controller chip to turn on. The bias voltage and set voltage will be provided by power supplies to simulate the 48V DC bus line providing the voltages to the LT1716 [12]. Figure 4-13 shows a circuit diagram of the first design.

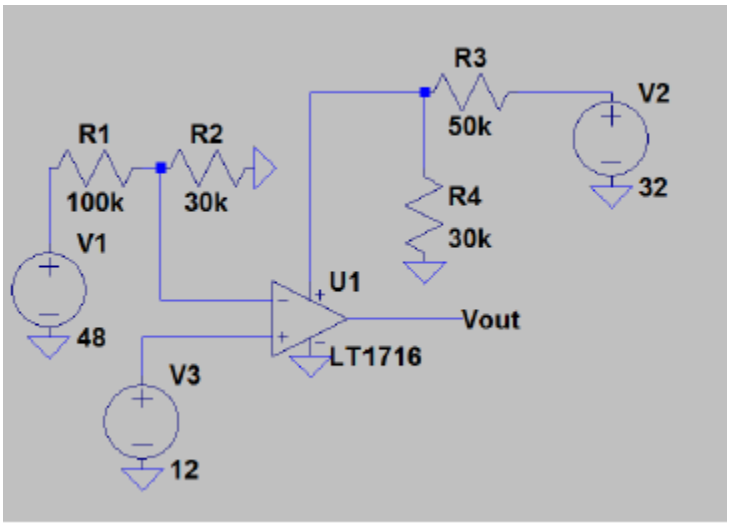

Figure 4-13: First Design of Bi-Directional Control Scheme [12]

With the current control scheme, the bi-directional converter is always either charging or discharging the lead-acid batteries. When the MISO converter that supplies the 48V DC bus line is operating, the bi-directional converter is also discharging the batteries. This can cause problems in situations when the battery has completely discharged during the day and the MISO converter stops operating but there is still a demand for energy from the house. A new control scheme will be developed to address this issue. The new design will allow the discharging stage to operate only when the DC bus line is not being supplied by the MISO converter.

The improved control scheme will utilize the same shutdown options as the first design, but will now detect the voltage levels at both the lead-acid battery and DC bus line. Two voltage level detectors will be implemented to monitor the voltage at the DC bus line and lead-acid battery terminals. The MISO converter that provides the DC bus line outputs an average voltage of 48.3V [20], while the bi-directional converter outputs an average voltage of around 48V. The minimum voltage that the battery will discharge

to, to avoid damaging the life of the battery, will be 11V. These three voltage levels will be used to determine the threshold for the detectors. When the voltage of the battery is above 11V and the DC Bus line is below 48.3V, the discharging stage will be activated. When the battery voltage drops to or below 11V, none of the converters will be allowed to operate. If the DC bus line voltage is at 48.3V or higher, the charging stage will activate charging the lead-acid battery. Table 4-3 provides a summary of the operating states of this control scheme.

Table 4-3: Bi-directional Control Scheme States

	DC Bus Line <48.3V	**DC Bus Line >48.3V**
Battery Voltage <11V	Do Nothing	Charge
Battery Voltage >11V	Discharge	Charge

The level detectors will be implemented using the LT1716 comparator and a LT1634-2.5 reference diode. The reference diode, when biased, provides an accurate 2.5V that the comparator will use to determine when the input voltages surpass the threshold voltage. A resistive divider connected to the input of the comparator will provide a voltage that is 2.5V at the desired threshold voltage. The output voltages of these level detectors will be processed using logic gates to drive the two stages of the bi-directional converters as specified in Table 4-3.

The flyback converter is an isolated topology meaning that the primary and secondary grounds are separated. The logic needed to drive the MOSFET switch for the shutdown of the discharging converter is dependent on the voltage level of the DC bus line. Therefore an opto-coupler with a photodiode output is required to accurately

monitor the voltage on the bus line with respects to the lead-acid battery ground. The Avago HCNR200 opto-coupler will be used for this purpose. In a photodiode output opto-coupler, as the input signal varies, it will vary the intensity of the infrared light of an LED. This induces a photo current to flow through the output diode. With a load resistor connected to the output terminals of the coupler, the photo current will develop a voltage across the load. As output current increases, output voltage also increases, and vice-versa [21]. Figure 4-14 shows how the opto-coupler operates.

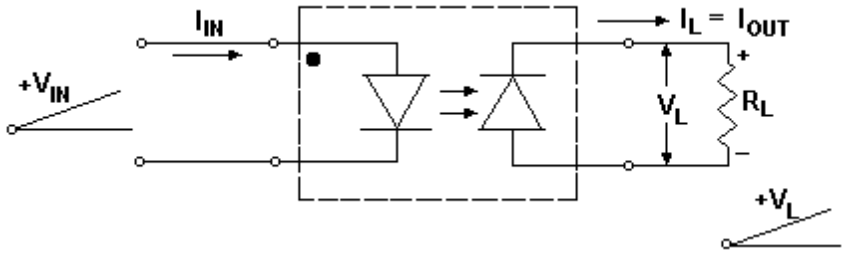

Figure 4-14: Opto-Coupler with Photo Diode Output [21]

The output voltage of the HCNR200 is in the mill-volts, so a non-inverting amplifier will be needed to increase the voltage to 2.5V when the DC bus line is at 48.3V. The HCNR200 also requires a maximum input current of 20mA to turn the LED on [22]. A 2.5kΩ is used to provide that current through the LED. The outputs of the control scheme will be 5V to bias the GATE of the shutdown MOSFETS connected in parallel to the resistive divider at the EN/UVLO pins of each controller. The chosen MOSFET for the shutdown feature is a Fairchild 2N7000TA which has a 3V gate-source biasing voltage. Figure 4-15 shows a complete schematic of the new control scheme.

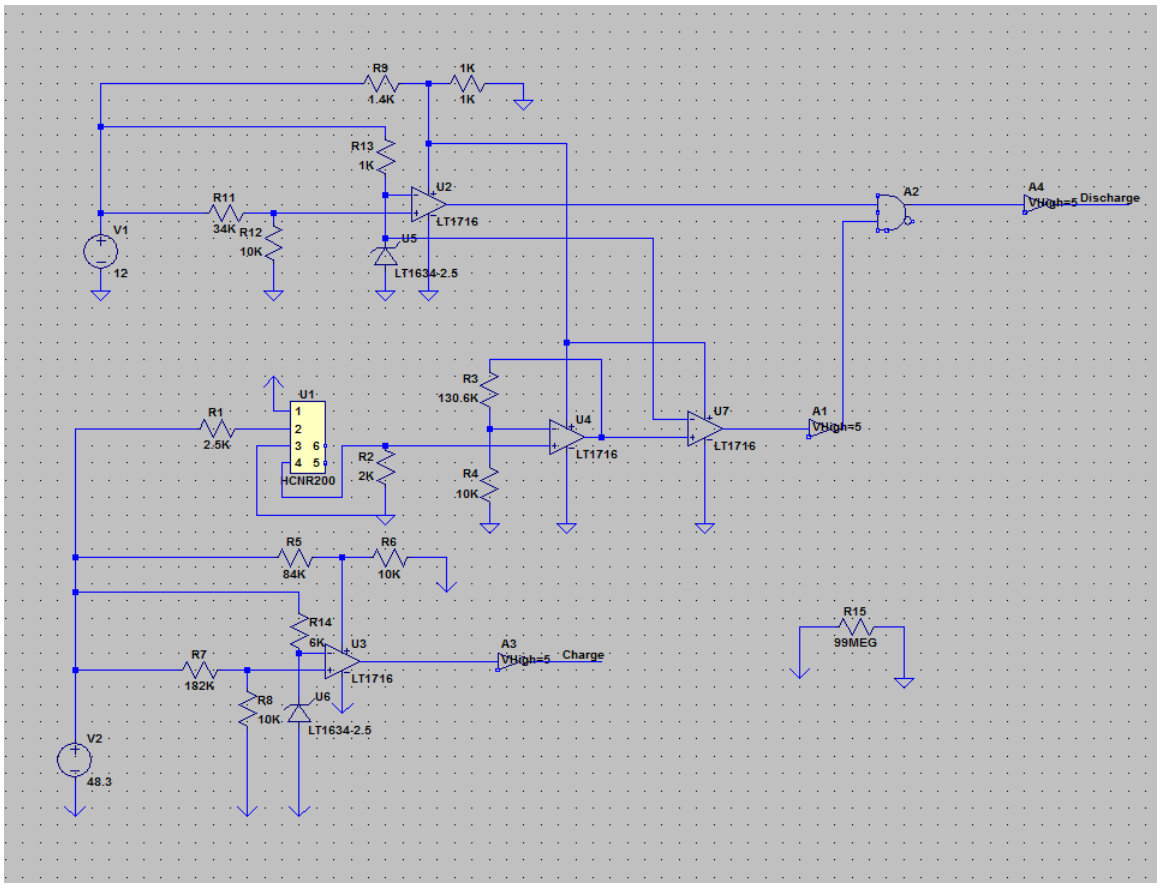

Figure 4-15: Improved Bi-Directional Control Scheme

Figures 4-16 to 4-19 shows the control scheme's output to the shutdown MOSFET for the charging and discharging LT3748 controller ICs under certain battery and bus line voltage levels. Signal V(charge) in blue is the output to the charging controller's shutdown MOSFET while signal V(discharge) in green is the output to the discharging controller's shutdown MOSFET. A high output voltage on the signal means the MOSFET is biases and the corresponding controller will be shutoff.

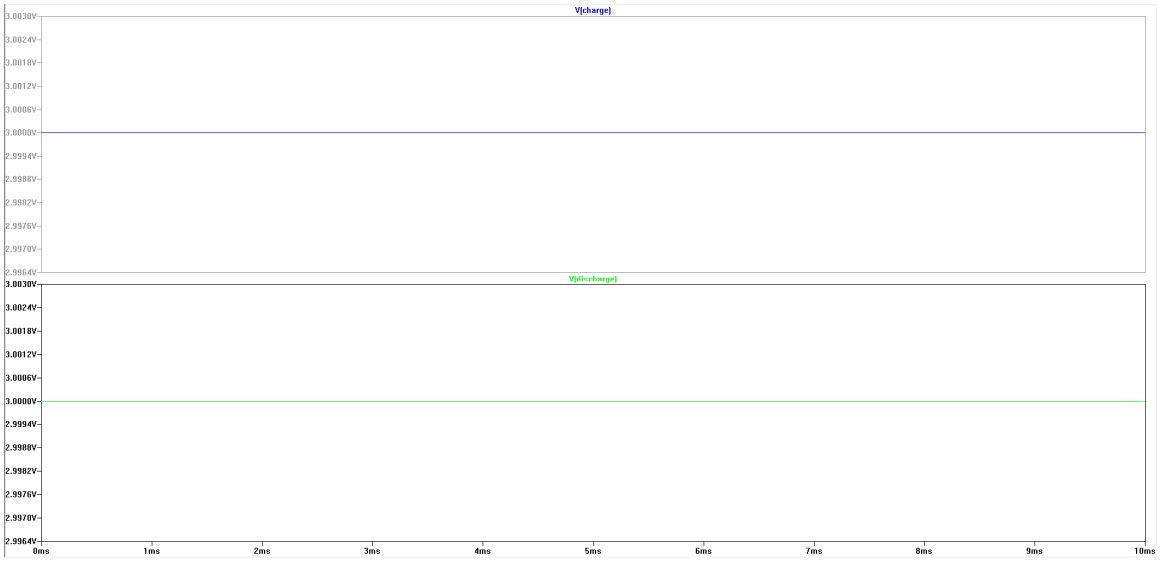

Figure 4-16: Output Voltage of Control Scheme when Battery Voltage is <11V and DC Bus Line <48.3V

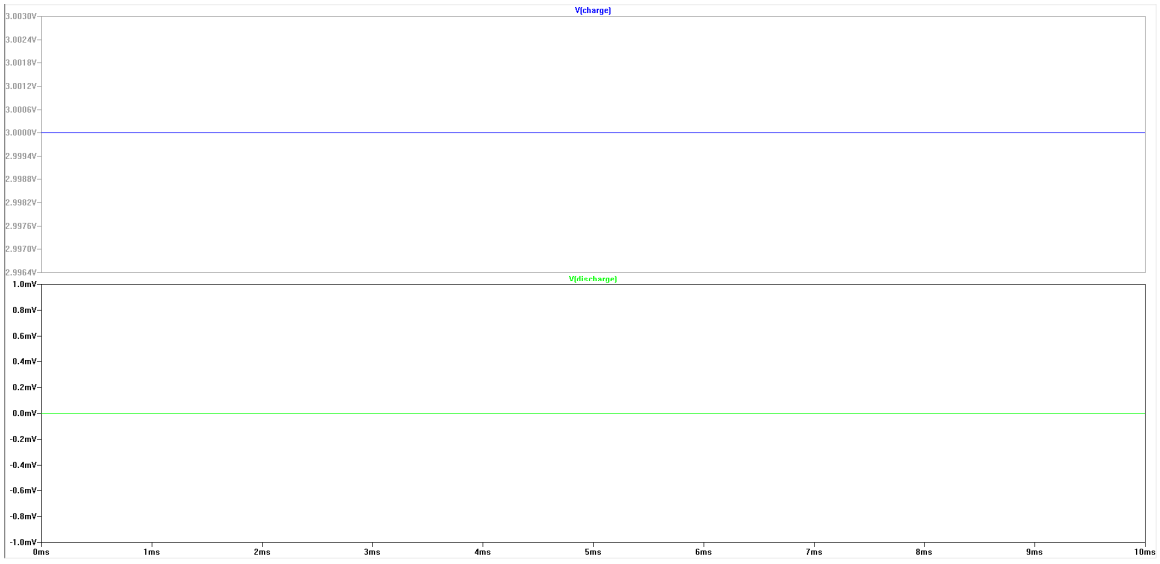

Figure 4-17: Output Voltage of Control Scheme when Battery Voltage is >11V and DC Bus Line <48.3V

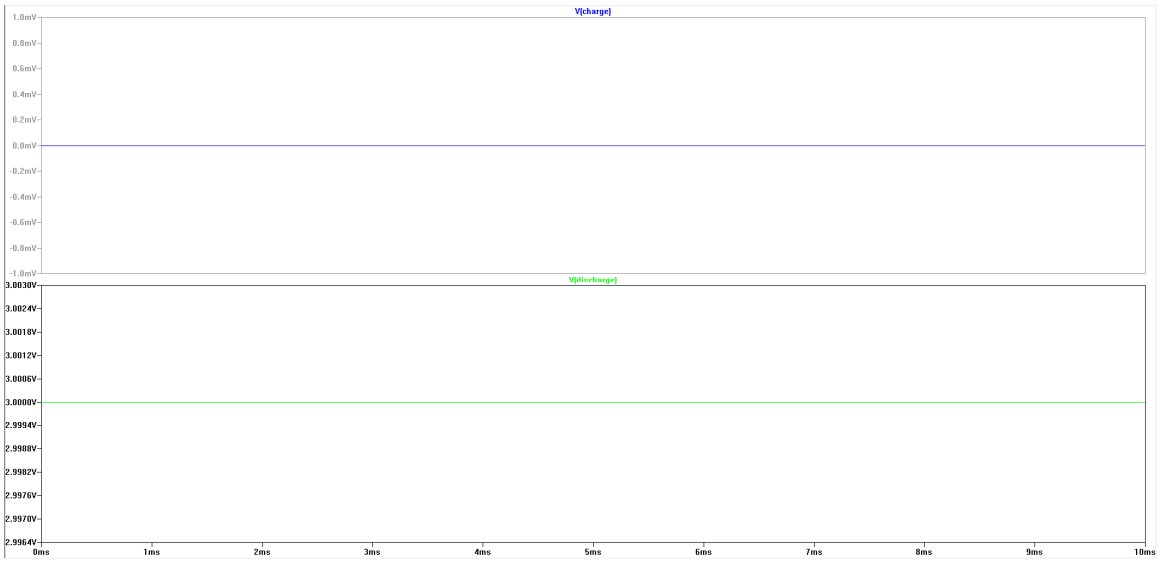

Figure 4-18: Voltage of Control Scheme when Battery Voltage is >11V and DC Bus Line >48.3V

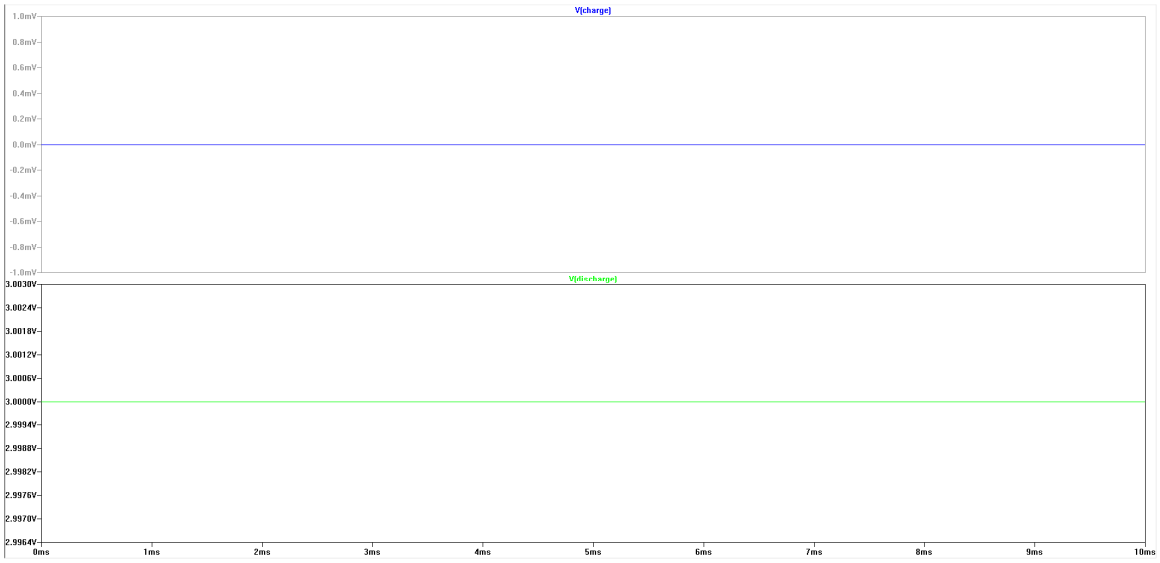

Figure 4-19: Voltage of Control Scheme when Battery Voltage is <11V and DC Bus Line >48.3V

4.7 Complete Bi-directional DC-DC Converter Design and Simulation Results

The complete schematic for the bi-directional DC-DC converter with control scheme is shown in Figure 4-20. To simulate each converter individually for efficiency, separate voltage sources will be added to the control scheme to emulate the battery and bus line voltages seen by the detectors.

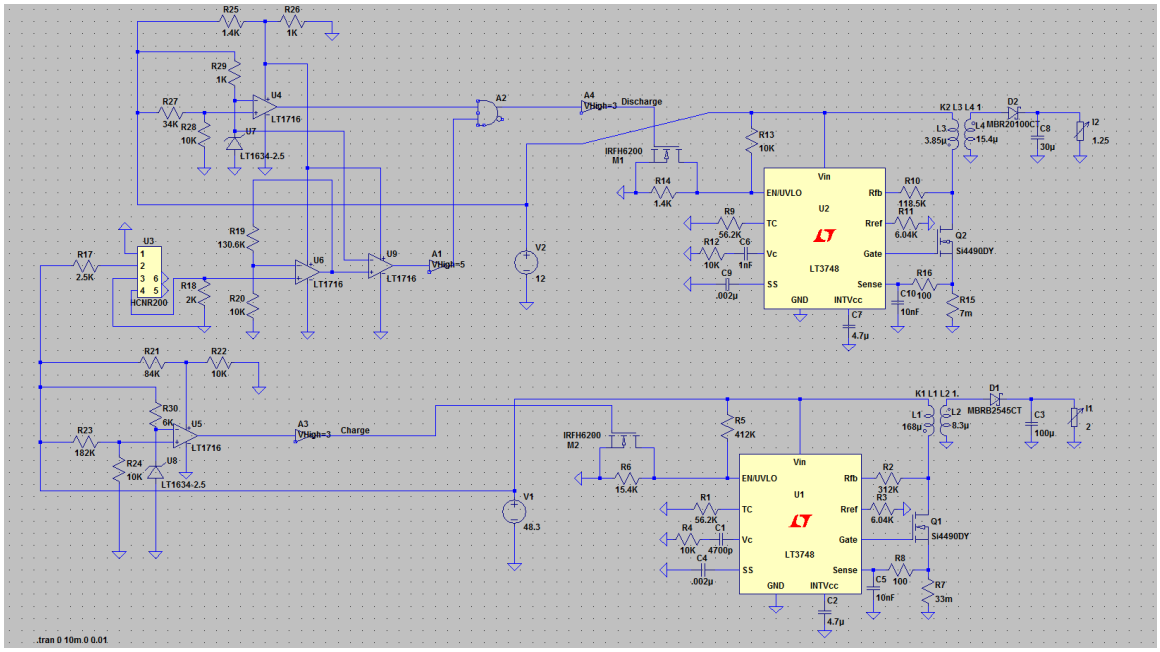

Figure 4-20: Complete Bi-Directional DC-DC Converter Schematic

Figure 4-21 shows the output voltage peak-to-peak ripple of the discharging flyback. The simulation output ripple of the discharging flyback at full load of 1.25A is 213.16mV or 0.44% of the output voltage.

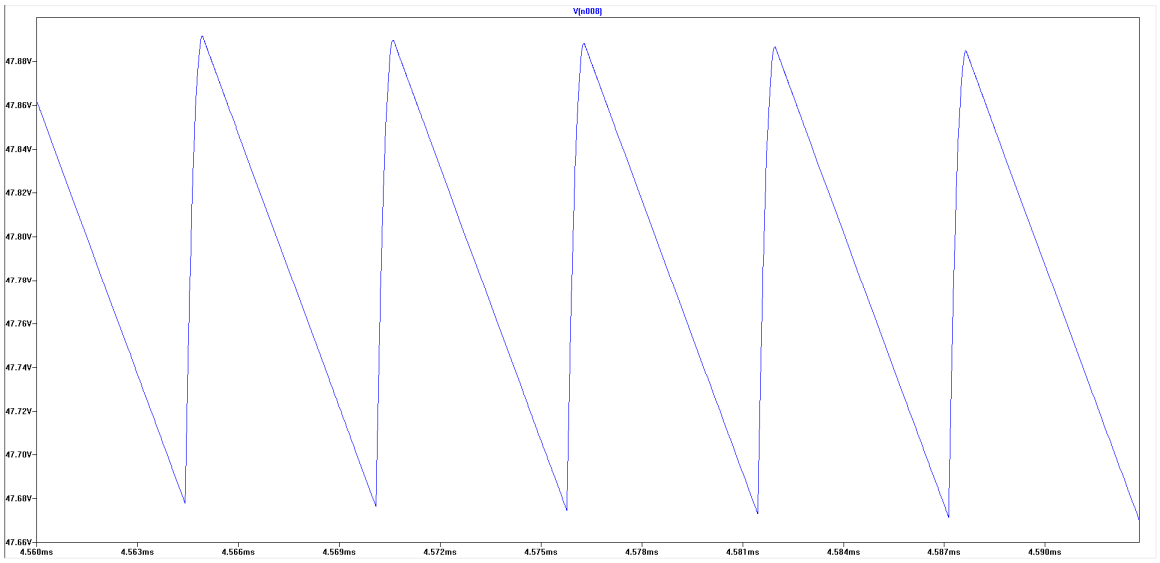

Figure 4-21: Simulation Output Ripple of Discharging Flyback

Figure 4-22 shows the gate voltages outputted by the LT3748 controller IC. The gate voltage of the discharging converter is pulsating while the charging converter is not. This is because the control scheme has shutdown the charging stage and allowed only the discharging stage to operate. Figure 4-23 shows the voltage at the sense pin of the discharging flyback.

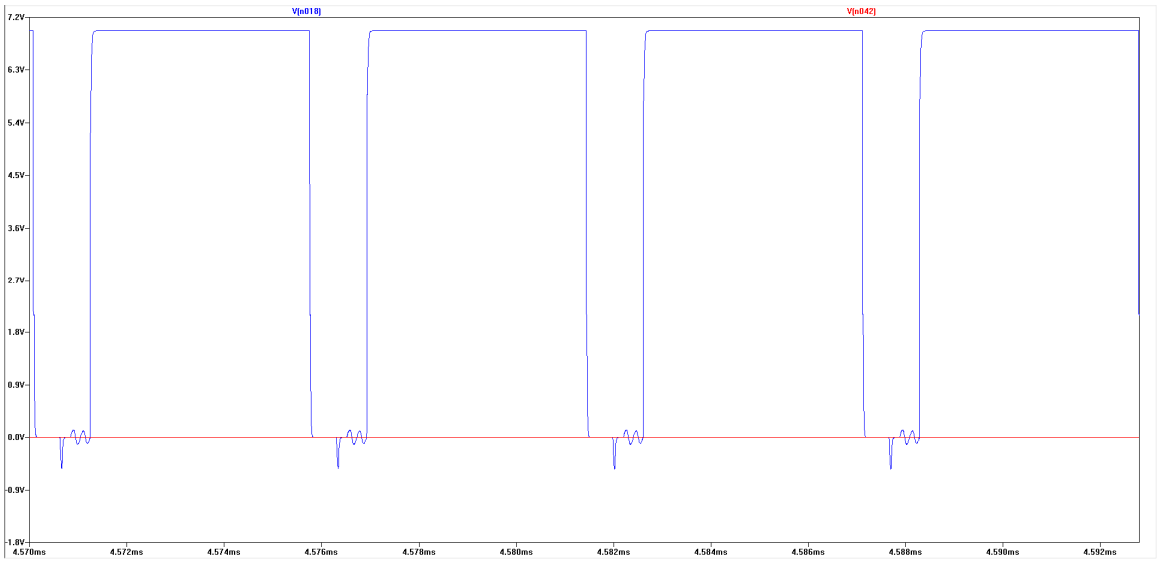

Figure 4-22: Gate Pin Voltages of LT3748 Control ICs (Discharging in Blue, Charging in Red)

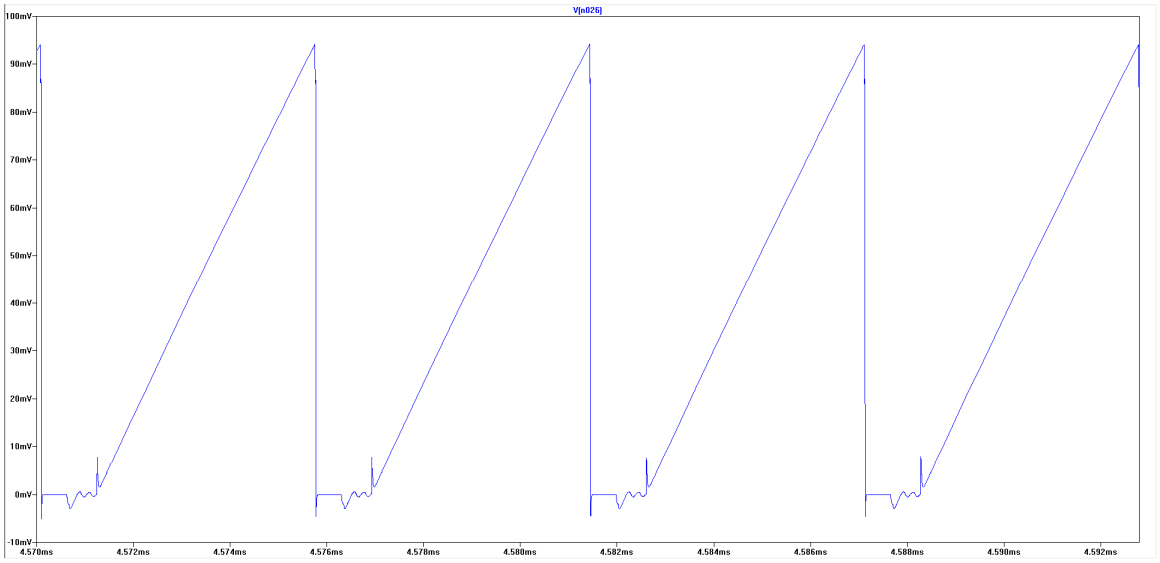

Figure 4-23: Sense Voltage of Discharging Flyback

Table 4-4 lists the simulation data recorded for output voltage and efficiency for the discharging flyback for a load current of 0.25A to 1.25A. The line and load regulations can be calculated using Equations 4.12 and 4.13 using the data from Table 4-4.

Table 4-4: Simulation Data of Discharging Flyback for Bi-Directional Converter

I_{in} (A)	I_{out} (A)	V_{in} (V)	V_{out} (V)	P_{in} (W)	P_{out} (W)	Eff %
5.51	1.25	12	47.78	66.06	59.72	90.41
4.39	1	12	47.80	52.79	47.80	90.56
3.33	0.75	12	47.93	39.92	35.94	90.05
2.25	0.5	12	48.19	26.95	24.09	89.41
1.22	0.25	12	50.07	14.59	12.51	85.73
6.01	1.25	11	47.76	66.12	59.70	90.29
5.08	1.25	13	47.79	65.98	59.74	90.54

The line regulation is determined to be 0.067% and the load regulation is determined to be 4.782%. The efficiency of the discharging flyback at various load currents is shown in Figure 4-24.

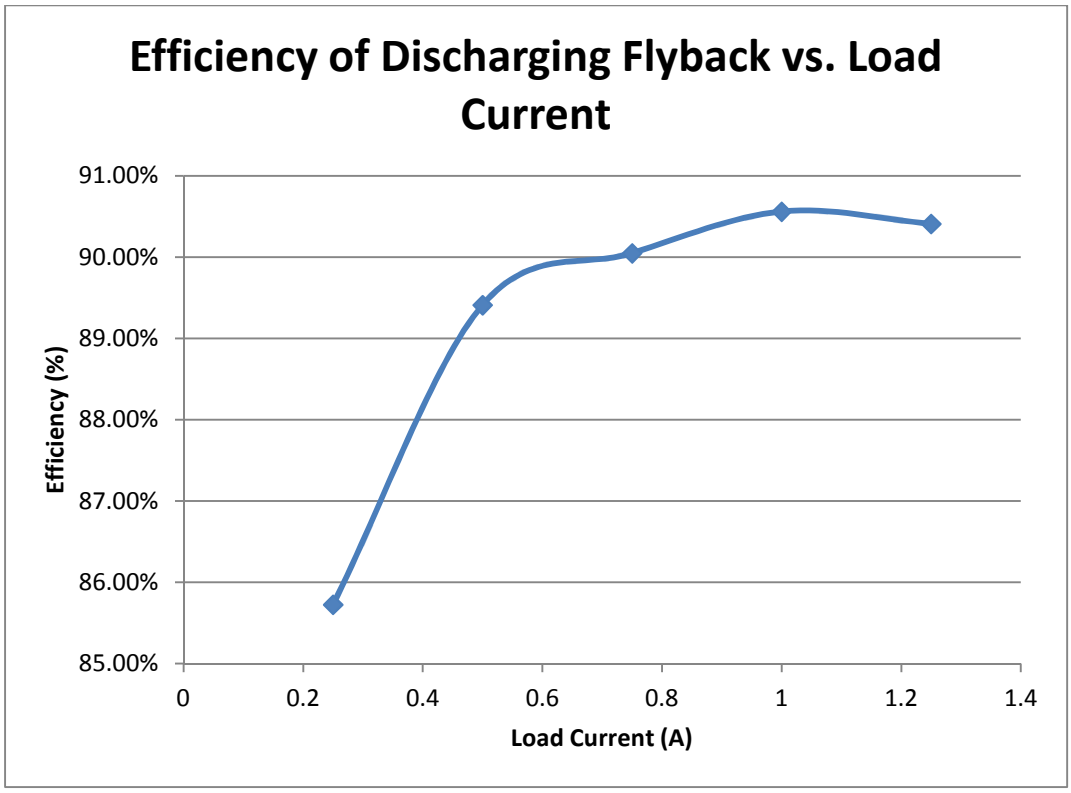

Figure 4-24: Efficiency of Discharging Flyback vs. Load Current for Bi-Directional Converter

Figure 4-25 shows the output voltage ripple of the charging flyback of the bi-directional converter. The output peak-to-peak ripple voltage is measured to be 181.91mV or 1.3% of the output voltage.

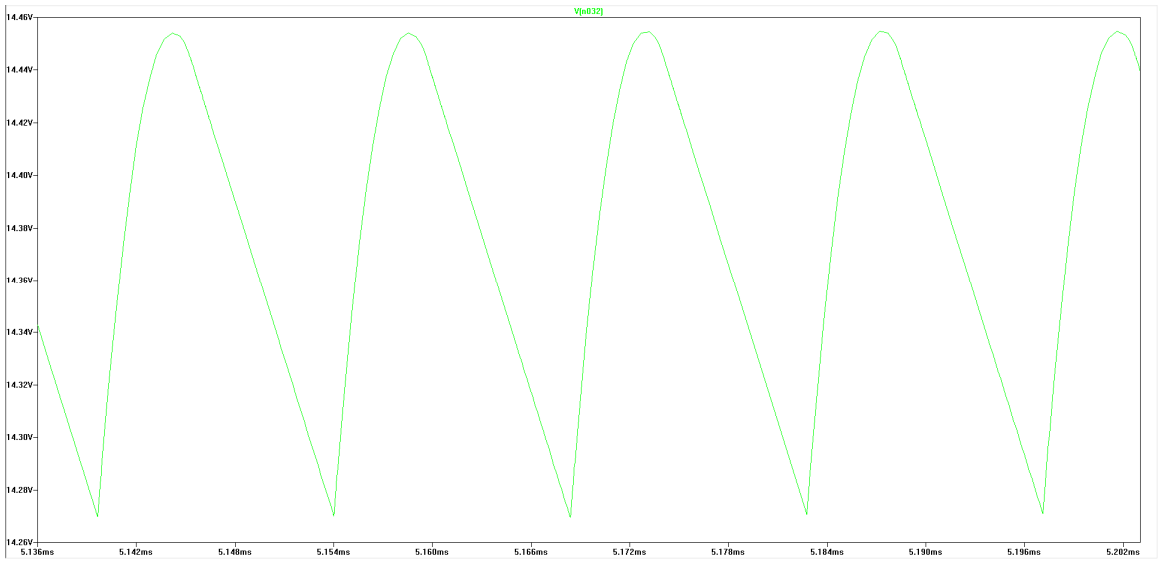

Figure 4-25: Simulated Output Ripple of Charging Flyback

Figure 4-26 shows the voltage of the gate pin for both LT3748 controller ICs. The gate voltage of the charging converter is pulsating while the discharging converter is not. This is because the control scheme has shutdown the discharging stage and allowed only the charging stage to operate. Figure 4-27 shows the voltage at the sense pin of the charging flyback.

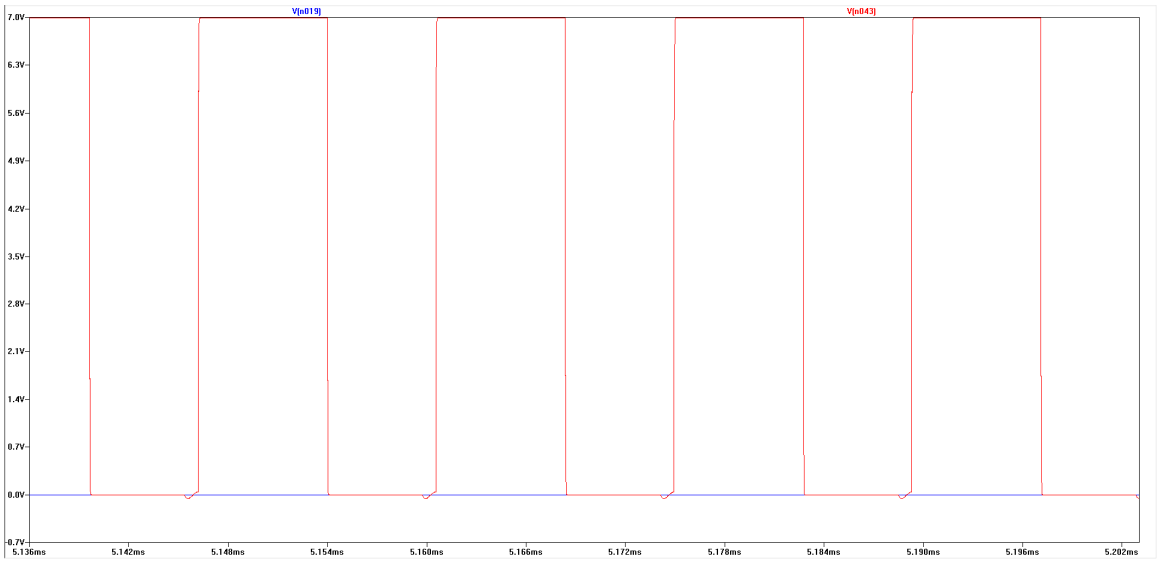

Figure 4-26: Gate Pin Voltages of LT3748 Control ICs (Discharging in Blue, Charging in Red)

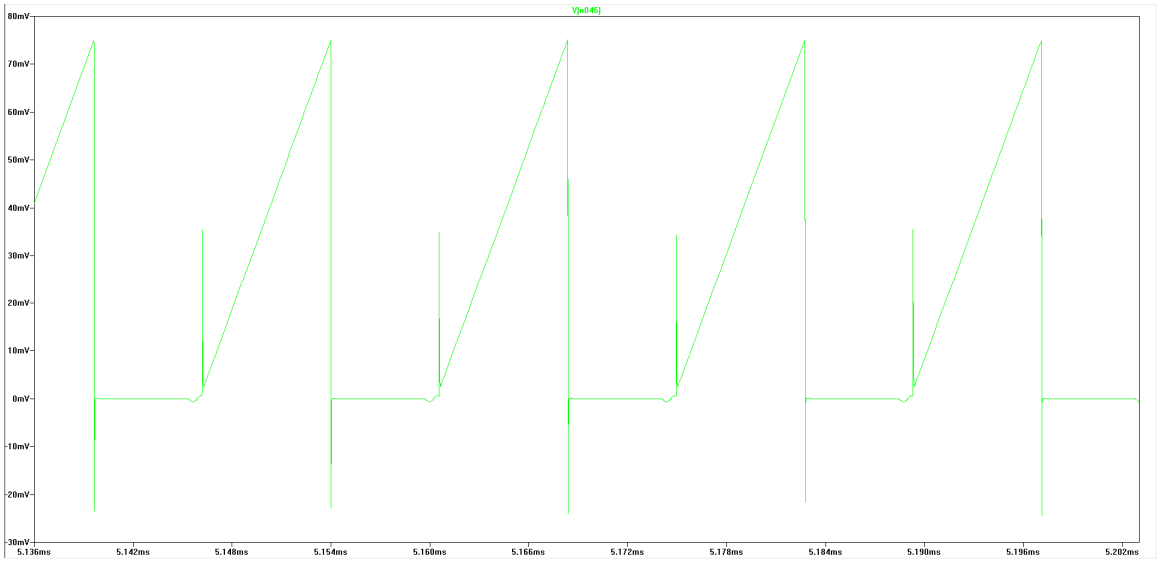

Figure 4-27: Sense Voltage of Charging Flyback

Table 4-5 lists the simulation data recorded for output voltage and efficiency for the charging flyback for a load current of 0.5A to 2A. The line and load regulations can be calculated using Equations 4.12 and 4.13 using the data from Table 4-5.

Table 4-5: Simulation Data of Charging Flyback for Bi-Directional Converter

I_{in} (A)	I_{out} (A)	V_{in} (V)	V_{out} (V)	P_{in} (W)	P_{out} (W)	Eff %
0.64	2	48	14.37	30.80	28.74	93.33
0.48	1.5	48	14.39	23.11	21.59	93.45
0.33	1	48	14.41	15.72	14.41	91.66
0.17	0.5	48	14.42	8.34	7.21	86.44
0.67	2	45.6	14.37	30.73	28.74	93.52
0.61	2	50.4	14.37	30.75	28.75	93.49

The line regulation is determined to be 0.028% and the load regulation is determined to be 0.341%. The efficiency of the charging flyback at various load currents is shown in Figure 4-28.

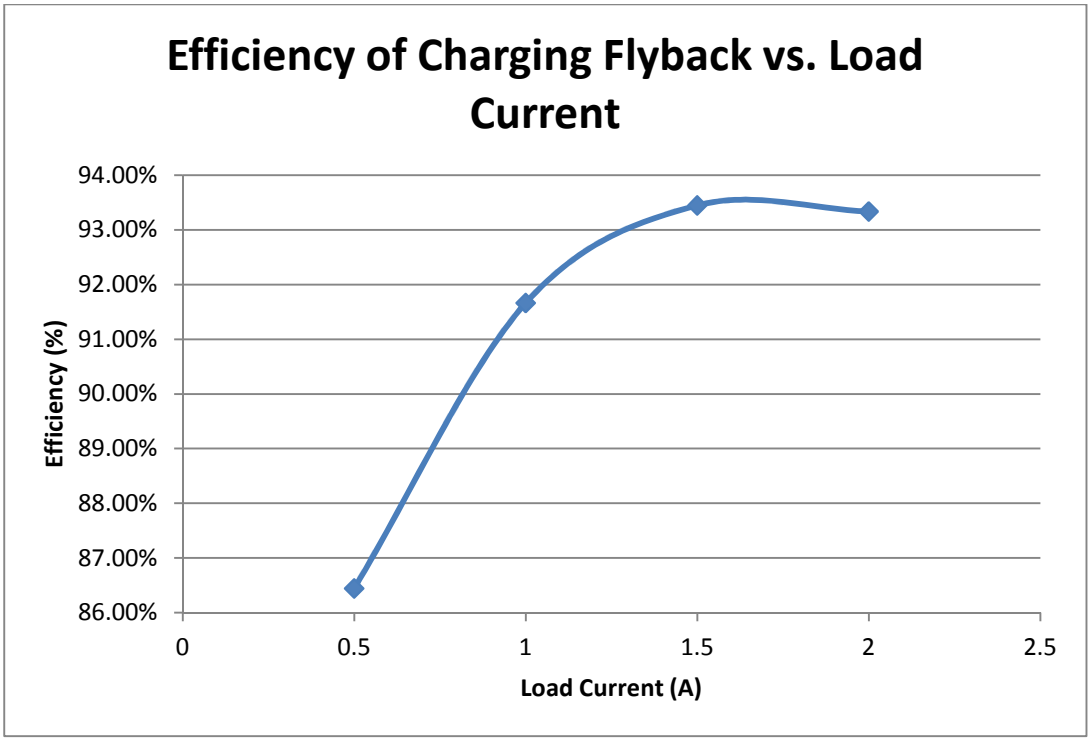

Figure 4-28: Efficiency of Charging Flyback vs. Load Current for Bi-Directional Converter

Table 4-6 summarizes and compares the simulation results for the bi-directional DC-DC converter to the design requirements listed in Chapter 3.

Table 4-6: Simulation Results and Design Requirements Comparison

	Charging Stage		Discharging Stage	
	Design Requirement	**Simulation Results**	**Design Requirements**	**Simulation Results**
Input Voltage	48V	48V	12V	12V
Output Voltage	14V	14.375V	48V	47.785V
Full Load Current	2A	2A	1.25A	1.25A
Full Load Output Power	28W	28.75W	60W	59.73W
Line Regulation	5%	0.028%	5%	0.067%
Load Regulation	5%	0.341%	5%	4.78%
Output Voltage Ripple	5%	1.30%	5%	0.44%
Efficiency at Full Load	≥80%	93.33%	≥80%	90.41%

With the data obtained in Table 4-6, the simulation results for both stages meet the design requirements outlined in Chapter 3.

4.8 Flyback Transformer Design

The LT3748 uses boundary conduction mode to provide current mode switching for the isolated flyback. However, designing the flyback transformer in continuous conduction mode covers boundary conduction operation and allows increased power capability for the bidirectional converter. Therefore, for the design of the transformer, continuous conduction mode considerations will be used [12].

Different types of core material exist that can be used for transformers. Each type has their own pros and cons, but the ferrite cores are ideal due to their low core cost and low core losses. Other types like tape wound cores offer higher flux densities and better temperature stability, but are much more costly [23]. Because the bi-directional converter is heavily focused on efficiency and cost, the ferrite core is chosen as the core material for the flyback transformer. Within the ferrite category, there are four types of cores that can be used. F, P, K and R material. Figure 4-29 shows core loss of different ferrite cores at different temperatures. The R material provides a lower core loss compared to the other materials. Thus, an R material ferrite core will be selected for the flyback transformers.

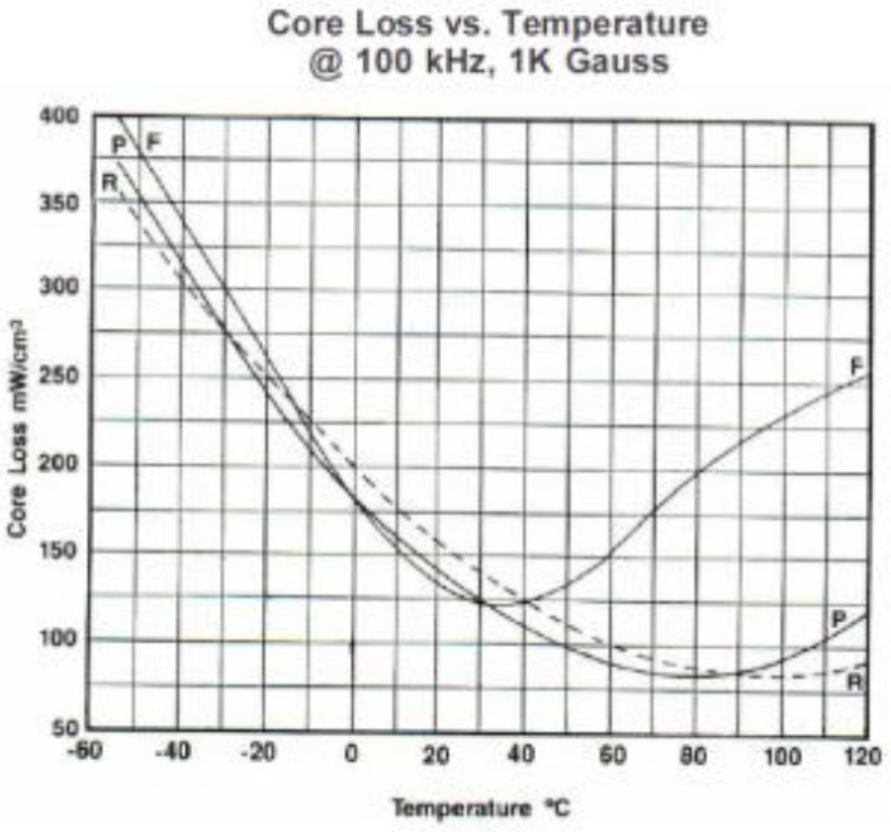

Figure 4-29: Core Loss vs. Temperature of Various Ferrite Core Materials [24]

The parameters for the charging and discharging flyback transformers are listed in Table 4-7. The first design for the converter used only one transformer, however due to the design changes in duty cycle and turns ratio, two separate transformers are needed.

Table 4-7: Charging and Discharging Flyback Design Parameters

	Charging Stage	Discharging Stage
Minimum Input Voltage	45.6V	11.4V
Maximum Input Voltage	50.4V	13V
Switching Frequency	100kHz	100kHz
Output Voltage	14V	48V
Output Power	28W	60W
Primary Inductance	168µH	4µH
Turns Ratio $\frac{N_P}{N_S}$	4	0.5

The area product method will be used to determine the minimum core size of the flyback transformers [25]. The area product is determined using Equation 4.16.

$$A_P = \left(\frac{L_P * I_{P(peak)} * I_{P(RMS)} * 10^4}{420 * k * B_{max}}\right) \tag{4.16}$$

A_P: Area product in cm^4

L_P: Primary Inductance in Henrys

$I_{P(peak)}$: Peak Primary Inductance Current in Amps

$I_{P(RMS)}$: Primary RMS Current in Amps

K: Winding Factor

B_{max}: Maximum Flux Density of Core Material in Tesla

The peak primary inductance current and primary RMS current can be calculated using Equations 4.17 and 4.18 [25].

$$I_{P(peak)} = \left(\frac{N_S}{N_P} * I_{o(\max)}\right) * \left(\frac{1}{1-D_{max}}\right) + \left(\frac{\Delta I_{LP}}{2}\right) \tag{4.17}$$

$$I_{P(RMS)} = \sqrt{\left(\frac{t_{on(\max)}}{T}\right) * \left(I_{P(peak)}^2 - \Delta I_{LP} * I_{P(peak)} + \frac{\Delta I_{LP}^2}{3}\right)} \tag{4.18}$$

D_{max}: Maximum Duty Cycle

ΔI_{LP}: Peak-to-peak Primary Inductance Current in Amps

$t_{on(max)}$: Maximum On-Time of Switch in seconds

The peak-to-peak current is determined using the following equation [25]:

$$\Delta I_{LP} = \frac{\Delta t * (V_{in(\min)} - V_{SW(on)})}{L_P} \quad (4.19)$$

Δt: Time that the primary inductance current is changing in seconds

$V_{in(min)}$: Minimum Input Voltage in Volts

$V_{SW(on)}$: Voltage drop across the switch in Volts

For the charging transformer, assuming Δt of 5.86µs, which is based on the duty cycle of 0.58 and a switching frequency of 100kHz, voltage drop of 1V across the switch when it is on, minimum input voltage of 45.6V, and a primary inductance of 168.2µH, the peak-to-peak current is calculated to be 1.55A. With this value, the peak primary inductance current can be determined. Assuming $\frac{1}{4}$ for $\frac{N_S}{N_P}$, a maximum output current of 2A, and maximum duty cycle of 0.58, Equation 4.17 equates to 1.98A. The RMS current of the primary inductance is then determined to be 0.98A. Using the values obtained from Equations 4.17-19, a winding factor of 0.2 for a flyback [25], and B_{max} of 0.47T for R Material [26], the area product for the charging flyback transformer core is 0.0829cm^4. This calculated area product provides a minimum value for the core size selection.

Using a table of R material ferrite cores and their corresponding area products, the PQ3535 core is chosen due to its large area product of 3.1cm^4 [27]. With the parameters of the chosen core show in Table 4-8, the minimum number of turns for the primary and secondary windings can be determined using the following equation [25]:

$$N_P = \frac{L_P * (I_{P(peak)} * 10^4)}{B_{max} * A_e} \quad (4.20)$$

N_P: Number of Turns of Primary Winding

A_e: Effective Core Area in cm^2

Table 4-8: PQ3535 Core Specifications [28]

PQ3535 Core Parameters					
A_p (cm^4)	A_e (cm^2)	μ_r	$\mu_o \left(\frac{H}{m}\right)$	L_m (cm)	r (cm)
3.1	1.9	2300	1.25E-6	8.61	0.72

Assuming primary inductance of 168.2µH, a peak primary current of 1.98A, a maximum flux density of 0.47T and an effective area product of $1.9cm^2$, the minimum number of turns for the primary winding is calculated to be 3.73 and considering the turns ratio of 4:1, the secondary winding will have a minimum of 0.93 turns. For easier implementation of the transformers, the number of turns of the primary will be rounded up to the nearest integer of 4 turns, which corresponds to 1 turn on the secondary.

Energy storage in a flyback transformer is done through the use of air-gaps. The high permeability of the ferrite material does not allow much energy to be stored without the core saturating first [25]. The air-gap length can be determined using the following equation [25]:

$$l_g = \frac{\mu_r * \mu_o * N_P^2 * A_e * 10^{-2}}{L_P} \quad (4.21)$$

l_g: Air-gap length in cm

μ_r: Relative Permeability of Core

μ_o: Permittivity of Free Space in $\frac{H}{m}$

From the datasheet for the PQ3535 core [28] and from Table 4-8, the relative permeability of core is 2300 and the permittivity of free space is $4\pi*10^{-7}$ H/m. Assuming a minimum primary winding with 4 turns and a primary inductance of 168.2µH, the air-gap length is $5.3*10^{-3}$ cm. The air-gap will be created using Kapton tape, which is 2 mil in length. Converting the calculated values to mil using a conversion ratio of $\frac{1mil}{0.00254cm}$, one layer of Kapton tape will be used to create the necessary air-gap.

Determining the proper wire gauge size for the primary and secondary windings will require the current density of the transformer. The following equation will provide the current density for the core [25]:

$$J = K_j * A_P^{-0.125} \tag{4.22}$$

J: Current density in $\frac{A}{cm^2}$

K_j: Current Density Coefficient

The current density coefficient is determined by the core type, in this case a PQ core is a pot core with a coefficient of 632 [25]. With an area product of $3.1cm^4$, the current density is calculated to be $862.7\frac{A}{cm^2}$. With the current density, the bare wire sizes for the primary and secondary windings can be established using the following equations [25]:

$$AWB_P = \frac{I_P}{J} \tag{4.23}$$

$$AWB_S = \frac{I_S}{J} \tag{4.24}$$

I_P: Average Primary Current in Amps

I_S: Average Secondary Current in Amps

The average primary current through the primary inductance is the input current which can be calculated by dividing the average input voltage (48V) by the output power (25W) times the expected efficiency of the converter (80%). The average primary current is 0.65A. The average secondary current is the average output current which is 2A. With these values, the bare wire size of the primary and secondary are $0.75*10^{-3}$ cm^2 and $2.32*10^{-3}$ cm^2 respectively. An additional 10% is added to the calculated wire sizes to provide a maximum value of $0.83*10^{-3}$ cm^2 for the primary and $2.55*10^{-3}$ cm^2 for the secondary. With these values, a 28AWG wire is selected for the primary winding and a 24AWG wire is selected for the secondary winding of the charging flyback transformer.

To minimize leakage inductance and resistances of the transformer, a multi-layer design for the primary and secondary windings is considered. Three wires will be wound in parallel for each winding creating a tri-filar coil.

For the discharging transformer, assuming Δt of 8.9μs, which is based on the duty cycle of 0.89 and a switching frequency of 100kHz, voltage drop of 1V across the switch when it is on, minimum input voltage of 11.4V, and a primary inductance of 3.85μH, the peak-to-peak current is calculated to be 24.07A. With this value, the peak primary inductance current can be determined. Assuming 2 for $\frac{N_S}{N_P}$, a maximum output current of 1.25A, and maximum duty cycle of 0.89, Equation 4.17 equates to 34.9A. The RMS current of the primary inductance is then determined to be 22.6A. Using the values obtained from Equations 4.17-19, a winding factor of 0.2 for a flyback [25], and B_{max} of 0.47T for R Material [26], the area product for the discharging flyback transformer core is $0.77cm^4$. This calculated area product provides a minimum value for the core size selection.

Using a table of R material ferrite cores and their corresponding area products, the PQ3535 core will also be used due to its large area product of 3.1cm^4 [27]. With the parameters of the chosen core show in Table 4-8, the minimum number of turns for the primary and secondary windings can be determined using the following equation [25]:

$$N_P = \frac{L_P*(I_{P(peak)}*10^4)}{B_{max}*A_e} \tag{4.20}$$

Assuming primary inductance of 3.85µH, a peak primary current of 34.9A, a maximum flux density of 0.47T and an effective area product of 1.9cm^2, the minimum number of turns for the primary winding is calculated to be 1.5 and considering the turns ratio of 1:2, the secondary winding will have a minimum of 3.01 turns. For easier implementation of the transformers, the number of turns on the primary will be rounded up to the nearest integer of 2 turns, which corresponds to 4 turns on the secondary.

Energy storage in a flyback transformer is done through the use of air-gaps. The high permeability of the ferrite material does not allow much energy to be stored without the core saturating first [25]. The air-gap length can be determined using the following equation [25]:

$$l_g = \frac{\mu_r*\mu_o*N_P^2*A_e*10^{-2}}{L_P} \tag{4.21}$$

From Table 4-8, the relative permeability of core is 2300 and the permittivity of free space is $4\pi*10^{-7}$ H/m. Assuming a minimum primary winding with 2 turns and a primary inductance of 3.85µH, the air-gap length is $21.1*10^{-3}$ cm. The air-gap will be created using Kapton tape, which is 2 mil in length. Converting the calculated values to mil using a conversion ratio of $\frac{1mil}{0.00254cm}$, two layers of Kapton tape will be used to create the necessary air-gap.

Determining the proper wire gauge size for the primary and secondary windings will require the current density of the transformer. The following equation will provide the current density for the core [25]:

$$J = K_j * A_P^{-0.125} \tag{4.22}$$

The current density coefficient is determined by the core type, in this case a PQ core is a pot core with a coefficient of 632 [25]. With an area product of 3.1cm^4, the current density is calculated to be 652.95$\frac{A}{cm^2}$. With the current density, the bare wire sizes for the primary and secondary windings can be established using the following equations [25]:

$$AWB_P = \frac{I_P}{J} \tag{4.23}$$

$$AWB_S = \frac{I_S}{J} \tag{4.24}$$

The average primary current through the primary inductance is the input current which can be calculated by dividing the average input voltage (12V) by the output power (60W) times the expected efficiency of the converter (80%). The average primary current is 6.25A. The average secondary current is the average output current which is 1.25A. With these values, the bare wire size of the primary and secondary are 9.57*10^{-3} cm^2 and 1.91*10^{-3} cm^2 respectively. An additional 10% is added to the calculated wire sizes to provide a maximum value of 10.5*10^{-3} cm^2 for the primary and 2.11*10^{-3} cm^2 for the secondary. With these values, a 22AWG wire is selected for the primary winding and a 24AWG wire is selected for the secondary winding of the discharging flyback transformer.

To minimize leakage inductance and resistances of the transformer, a multi-layer design for the primary and secondary windings is considered. Three wires will be wound in parallel for each winding creating a tri-filar coil.

Table 4-9 summarizes the wire sizes and inductances for the charging and discharging flyback transformers.

Table 4-9: Wire Gauges and Inductances of Charging and Discharging Transformers

	Charging Transformer		Discharging Transformer	
	Primary Winding	**Secondary Winding**	**Primary Winding**	**Secondary Winding**
Inductance (µH)	168	8.3	4	16
Minimum Turns	4	1	2	4
Gauge Wire	28AWG	24AWG	22AWG	24AWG
Layers	3	3	3	3

Chapter 5 – Hardware Results

In this chapter, the results obtained from physical implementation of the design discussed in Chapter 4 will be analyzed in comparison with the design requirements of Chapter 3 and simulation results. The PCB layout for the converter and hardware results from testing of the charging and discharging stages will be shown in this chapter.

5.1 Flyback Transformers

As mentioned in Chapter 4, the flyback transformers will utilize the PQ3535 ferrite core. For both transformers, the primary winding will be wound around the bobbin first and then the secondary winding. The primary and secondary windings will be isolated from each other with three layers of Kapton tape. Besides isolation, the Kapton tape will make sure the windings are held tightly around the bobbin.

For the charging flyback transformer, the primary winding and secondary winding use three 28AWG and 24AWG wires, respectively, in parallel to split the current flow in order to improve efficiency and lower the leakage inductance of the transformer. The primary winding consists of four turns and the secondary winding has one turn. Figure 5-1 shows the completed charging flyback transformer.

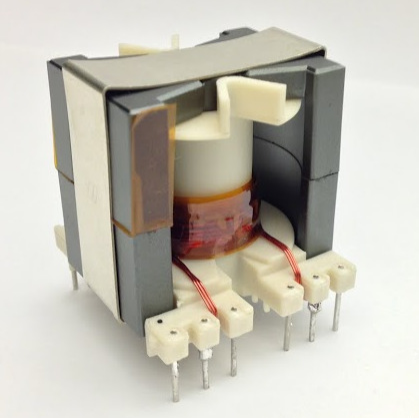

Figure 5-1: Charging Flyback Transformer for Bi-directional Converter

A sinusoidal waveform was used to verify dot terminals of the primary and secondary windings as well as the turns ratio. Figure 5-2 shows the resulting output of the transformer with a sinusoidal input. The peak-peak voltage of the input is 4.125V and the output voltage is 1V which corresponds to a 4.125:1 transformer. Figures 5-3 and 5-4 show the primary and secondary inductance values measured at a frequency of 100kHz. The primary inductance is measured to be 168.22µH and the secondary inductance is measured to be 8.26µH. The corresponding turns ratio can also be calculated from the transformer inductances using the following equation [25]:

$$\frac{N_1}{N_2} = \sqrt{\frac{L_1}{L_2}} \tag{5.1}$$

N_1 : Number of turns on primary winding

N_2: Number of turns on secondary winding

L_1: Primary Inductance in Henrys

L_2: Secondary Inductance in Henrys

By substituting the correct values for L_1 and L_2, the turns ratio of $\frac{N_1}{N_2}$, is calculated to be 4.51:1. The inductance values of the charging transformer matches closely to the desired values described in Chapter 4.

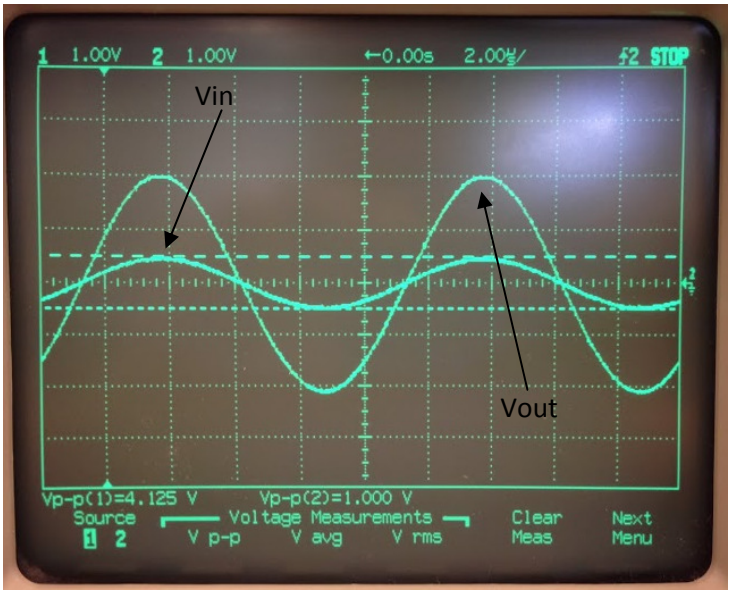

Figure 5-2: Input and Output Voltage Waveforms for Charging Flyback Transformer

Figure 5-3: Primary Inductance of Charging Flyback Transformer at 100 kHz

Figure 5-4: Secondary Inductance of Charging Flyback Transformer at 100 kHz

For the discharging flyback transformer, the primary winding and secondary winding uses three 22AWG and 24AWG wires, respectively, in parallel to split the current flow in order to improve efficiency and lower the leakage inductance of the transformer. The primary winding consists of two turns and the secondary winding has four turns. Figure 5-5 shows the completed discharging flyback transformer.

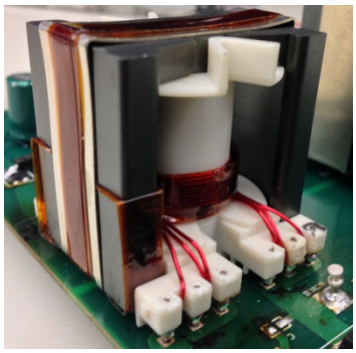

Figure 5-5: Discharging Flyback Transformer for Bi-directional Converter

A sinusoidal waveform was again used to verify dot terminals of the primary and secondary windings as well as the turns ratio. Figure 5-6 shows the resulting output of the transformer with a sinusoidal input. The peak-peak voltage of the input is 1V and the output voltage is 1.328V which corresponds to a 1:1.328 transformer. Figures 5-7 and 5-8 show the primary and secondary inductance values measured at a frequency of 100kHz. The primary inductance is measured to be 3.85µH and the secondary inductance is measured to be 8.96µH. The corresponding turns ratio can also be calculated from the transformer inductances using equation 5.1, which equates to a turns ratio of 1:1.52. Although the turns ratio is slightly lower than the desired 1:2, the primary inductance requirement of the controller is still satisfied.

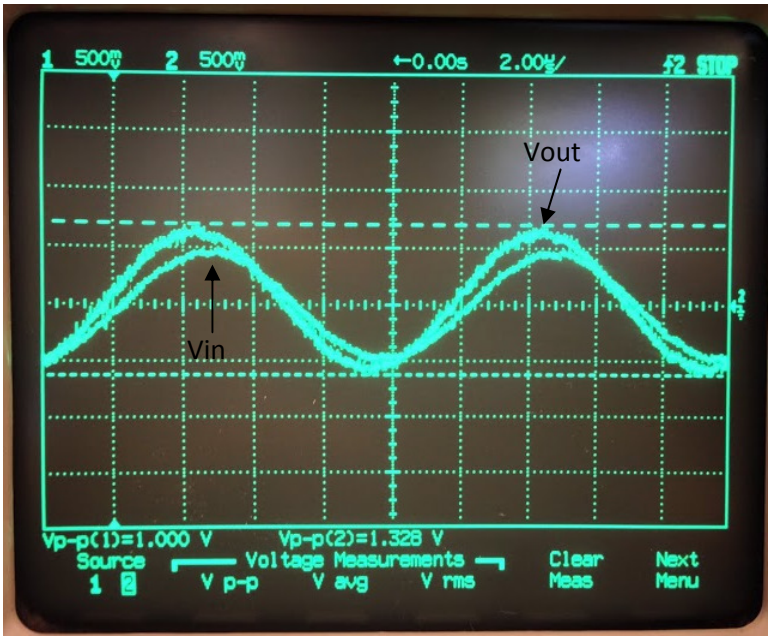

Figure 5-6: Input and Output Voltage Waveforms for Discharging Flyback Transformer

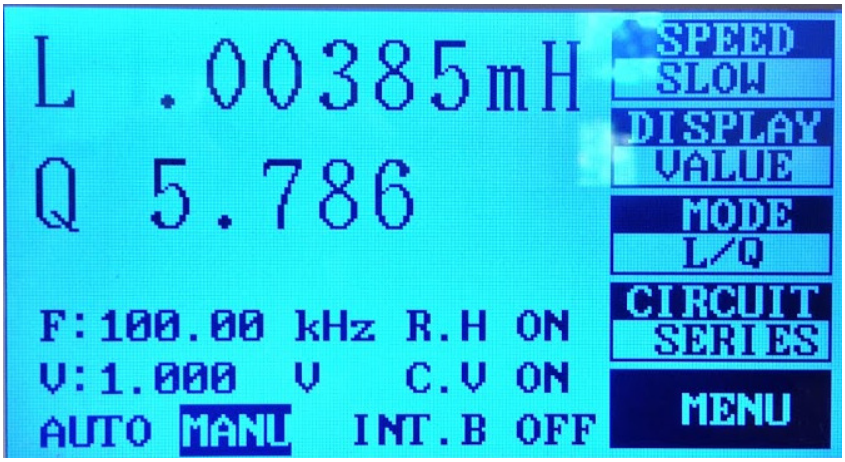

Figure 5-7: Primary Inductance of Discharging Flyback Transformer at 100kHz

Figure 5-8: Secondary Inductance of Discharging Flyback Transformer at 100 kHz

5.2 Bi-Directional DC-DC Converter PCB Layout

The circuit board layout of the bi-directional converter was designed using software provided by ExpressPCB. The board uses four layers: top copper layer, power layer, ground layer, and bottom copper layer. The top layer of the PCB is shown in Figure 5-9. The top layer is primarily for the two converters with the discharging on top and the charging on the bottom. The input voltage pins for each controller is tied to the power plane using vias. All ground connections are also connected to the ground plane using vias. Test points for the gate and drain of each MOSFET were added to easily monitor the signals at those nodes.

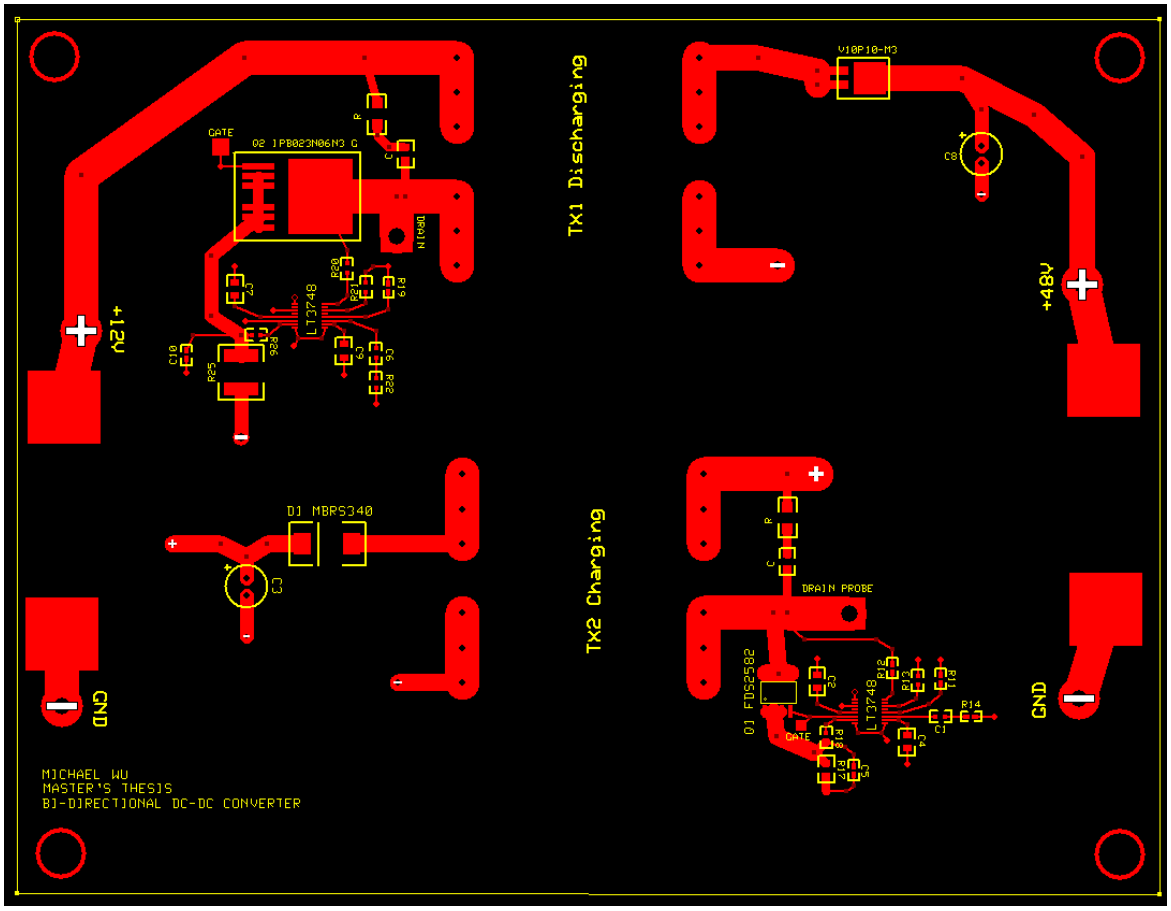

Figure 5-9: PCB Layout of Bi-Directional Converter

The control scheme for the bi-directional converter was prototyped on a copper clad board to allow for easier troubleshooting. Figure 5-10 shows the layout of for the control scheme. Pads for the inputs of the control board are provided for 12V and 48V. Outputs of the control board will be routed back to the EN/UVLO pin of each LT3748 IC.

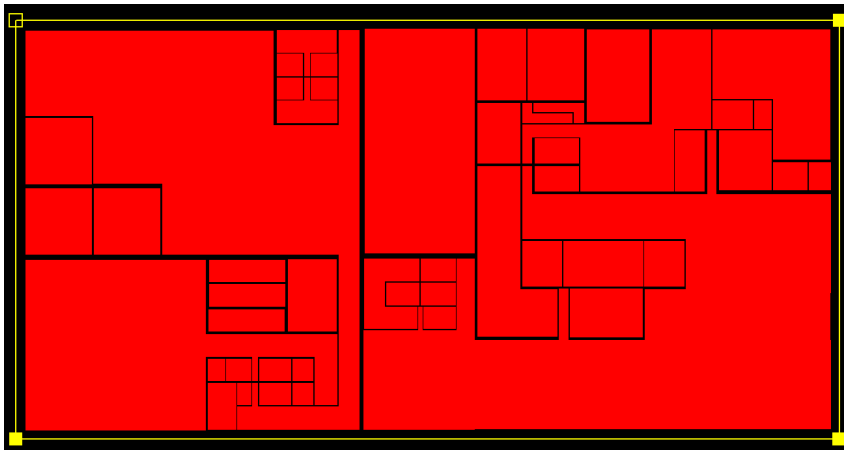

Figure 5-10: Board Layout for Control Scheme

5.3 Bi-Directional DC-DC Converter Test Setup

Figure 5-11 shows the testing set-up used for the bi-directional converter. The main input power supply is connected to two multimeters; one in series to monitor input current, and one in parallel to monitor input voltage. A separate 12V and 48V source is connected to the input of the control board to simulate the battery and DC bus line voltages. The output of the converter is connected to an electronic load which will control the output current of the converter. Two multimeters will be connected to the output; one in series to monitor output current, and one in parallel to monitor output voltage. Using separate multimeters to monitor voltage and current will give a more accurate reading to calculate input and output power. An oscilloscope will be used to monitor specific voltage waveforms of the converter.

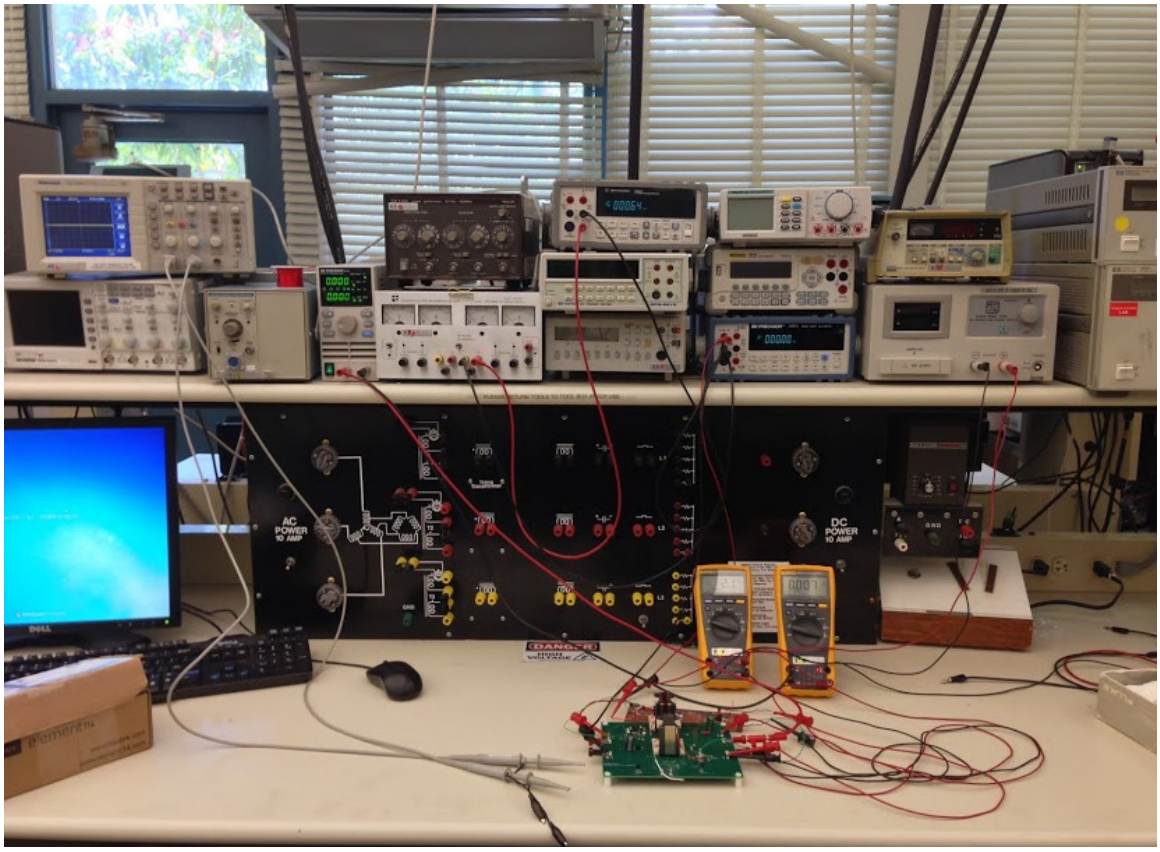

Figure 5-11: Testing Set-up for Bi-Directional Converter

5.4 Bi-Directional DC-DC Converter Charging Stage Hardware Results

The full load current of the charging flyback will be 2A at a regulated output voltage of 14V. Efficiency will be monitored from load currents of 0.1A to 2A in increments of 0.1A. The output voltage ripple, gate and drain voltage as well as sense voltage will be documented at full load. Table 5-1 shows the output voltages and efficiencies of the charging flyback for load currents of 0.1A to 2A.

Table 5-1: Output Voltages and Efficiency Data for Charging Flyback

I_{out} (A)	V_{out} (V)	P_{out} (W)	I_{in} (A)	V_{in} (V)	P_{in} (W)	Eff (%)
0.1	14.55	1.46	0.05	48.0	2.18	67.00
0.2	14.53	2.91	0.08	48.0	3.93	73.90
0.3	14.53	4.36	0.12	48.0	5.61	77.70
0.4	14.53	5.81	0.15	48.0	7.23	80.40
0.5	14.53	7.27	0.18	48.0	8.88	81.90
0.6	14.54	8.73	0.22	48.0	10.56	82.60
0.7	14.55	10.19	0.26	48.0	12.26	83.10
0.8	14.55	11.65	0.29	48.0	13.97	83.40
0.9	14.56	13.11	0.33	48.0	15.71	83.40
1.0	14.56	14.59	0.36	48.0	17.48	83.50
1.1	14.56	16.06	0.40	48.0	19.28	83.30
1.2	14.57	17.54	0.44	48.0	21.04	83.30
1.3	14.57	19.00	0.48	48.0	22.97	82.70
1.4	14.57	20.47	0.51	48.0	24.68	82.90
1.5	14.57	21.95	0.55	48.0	26.62	82.40
1.6	14.57	23.40	0.59	48.0	28.33	82.60
1.7	14.57	24.86	0.63	48.0	30.17	82.40
1.8	14.57	26.32	0.66	48.0	31.89	82.50
1.9	14.56	27.79	0.70	48.0	33.68	82.50
2.0	14.56	29.23	0.74	48.0	35.47	82.40
2.0	14.56	29.12	0.77	45.7	35.19	82.75
2.0	14.54	29.08	0.70	50.4	35.28	82.43

The average output voltage at full load is 14.56V. The drop in output voltage can be attributed to switching and copper losses. The input power and output power are calculated using the voltages and current measured from the multimeters. The line regulation is calculated using Equation 5.2 shown below:

$$Line\ Regulation = \frac{V_{out(hi-input)} - V_{out(lo-input)}}{V_{out(nom-input)}} * 100\% = \frac{14.56V - 14.54V}{14.56V} * 100\% = 0.137\% \quad (5.2)$$

Load regulation is calculated using Equation 5.3 shown below:

$$Load\ Regulation = \frac{V_{out(min-load)} - V_{out(max-load)}}{V_{out(max-load)}} * 100\% = \frac{14.55V - 14.56V}{14.56V} * 100\% = 0.068\% \quad (5.3)$$

Efficiency of the converter was calculated using Equation 5.4 shown below:

$$\eta = \frac{P_{out}}{P_{in}} * 100\% \quad (5.4)$$

The line and load regulations of the charging flyback are well below the required 5%. Figure 5-12 shows a graph of the efficiency of the charging stage for the bi-directional converter versus load current.

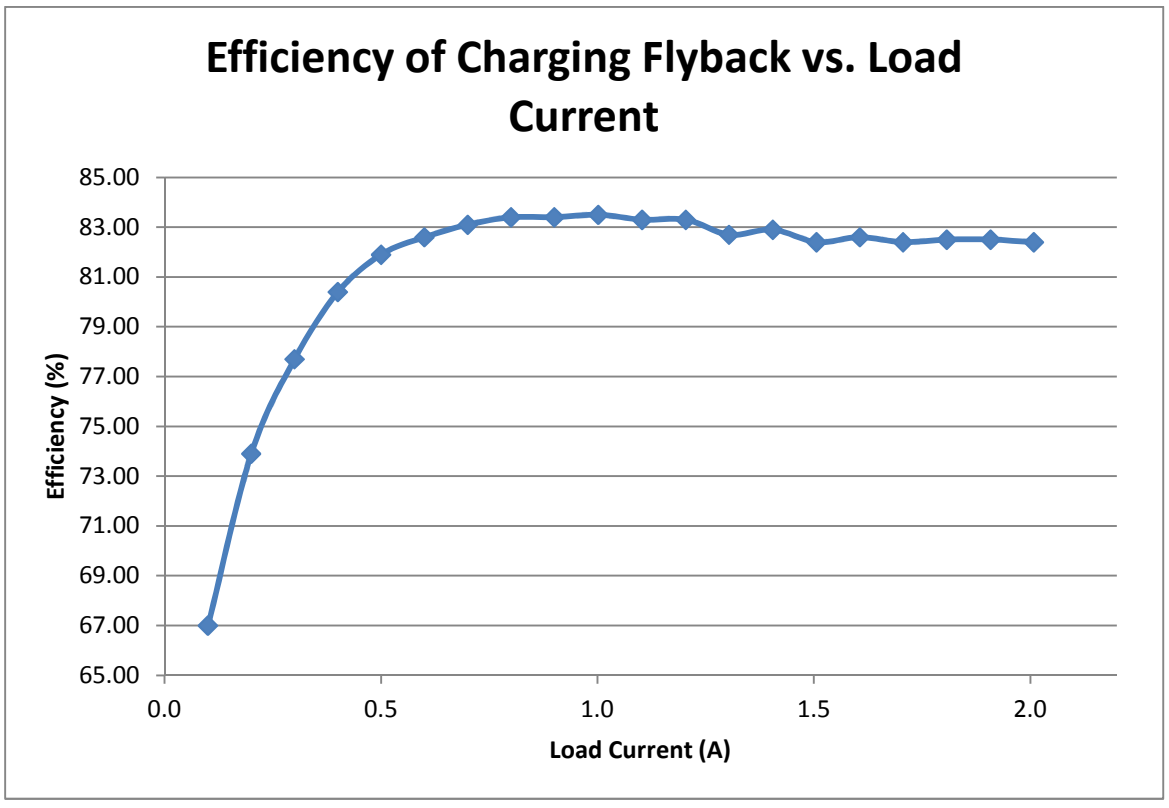

Figure 5-12: Efficiency vs. Load Current for Charging Stage

Figure 5-13 and Figure 5-14 shows the voltage waveform at the gate pin of the charging LT3748 IC and the drain voltage seen at the MOSFET of the charging stage at full load conditions respectively. Figure 5-15 shows the voltage at the sense pin of the charging LT3748 and Figure 5-16 shows the output voltage peak-to-peak ripple at full load conditions.

The output voltage peak-to-peak ripple at full load of 2A measures to be 212mV. The percentage of the output voltage that this ripple corresponds to can be calculated using Equation 5.5 below:

$$\%\frac{\Delta V}{V_o} = \frac{212V}{14.56V} * 100\% = 1.46\% \tag{5.5}$$

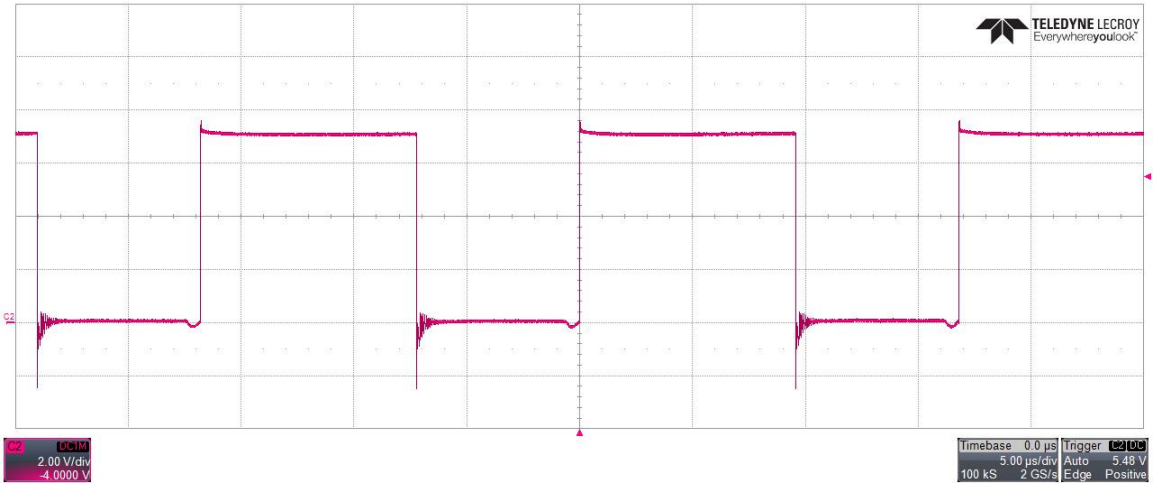

Figure 5-13: Gate Voltage of Charging Stage LT3748

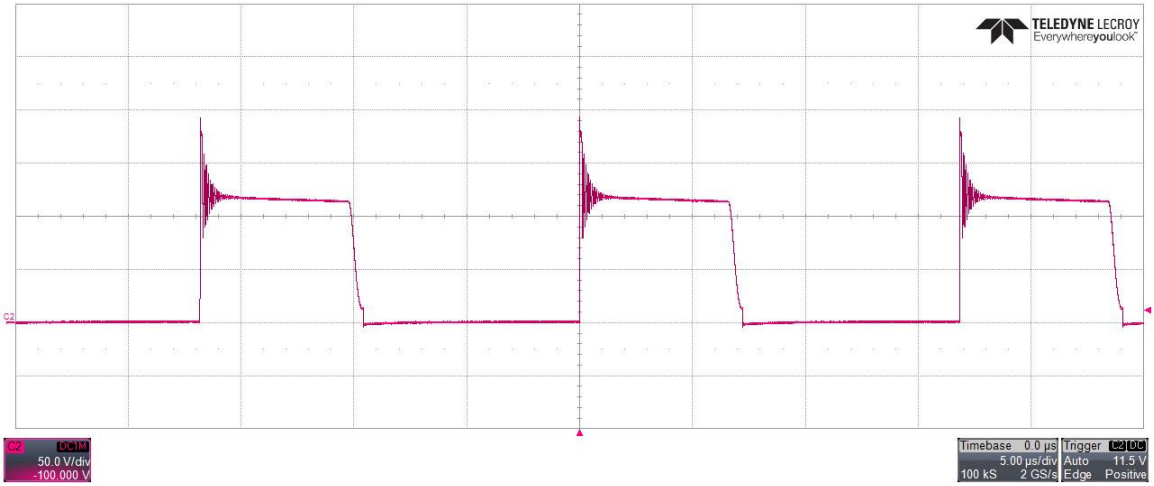

Figure 5-14: Drain-Source Voltage of Charging Stage MOSFET

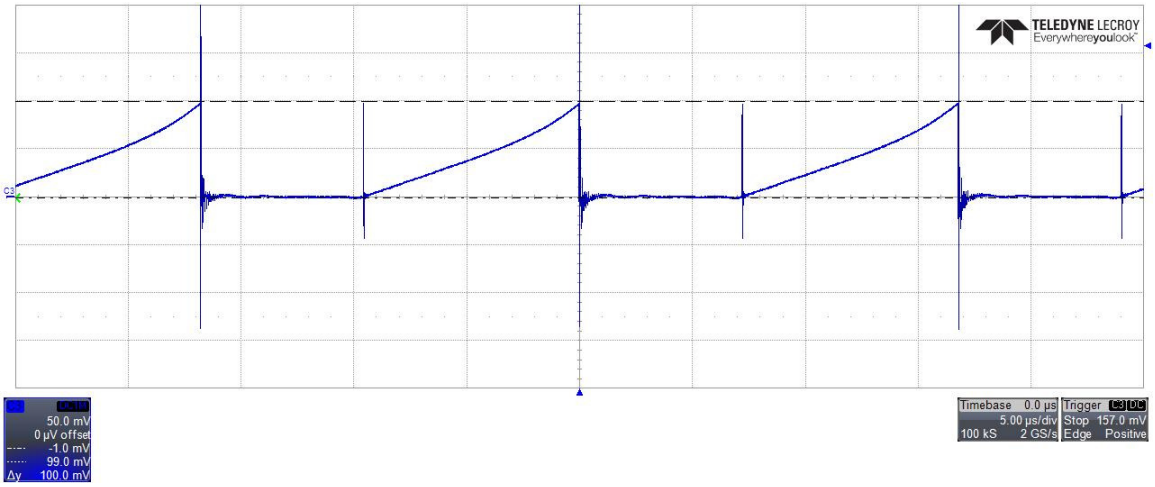

Figure 5-15: Sense pin of Charging Stage LT3748

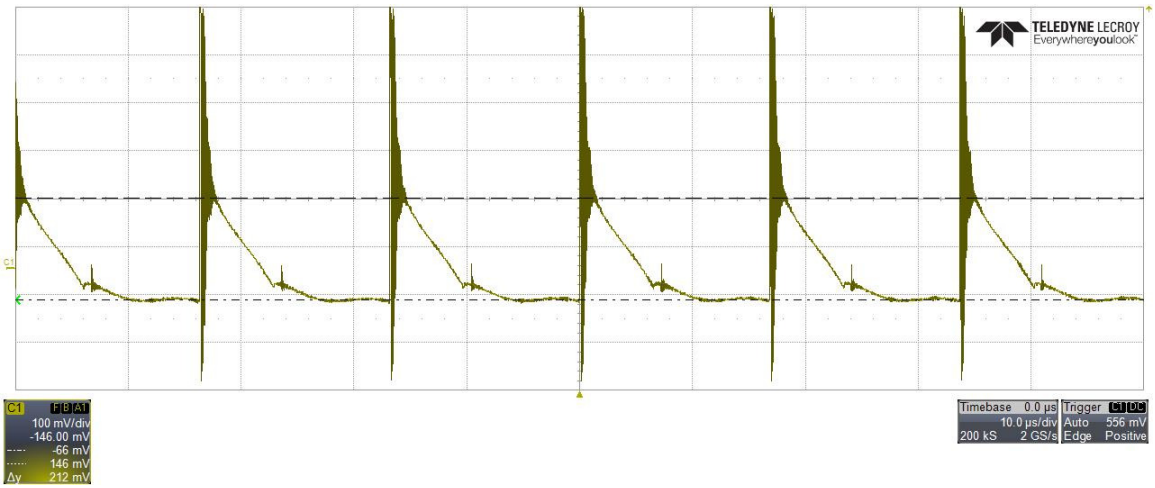

Figure 5-16: Output Voltage Peak-to-Peak Ripple of Charging Stage

5.5 Bi-Directional DC-DC Converter Discharging Stage Hardware Results

The full load current of the discharging flyback is 1A at a regulated output voltage of 47.8V. Efficiency will be monitored from load currents of 0.1A to 1A in increments of 0.1A. The output voltage ripple, gate and drain voltage as well as sense voltage will be documented at full load. Table 5-2 shows the output voltages and efficiencies of the discharging flyback for load currents of 0.1A to 1A.

Table 5-2: Output Voltages and Efficiency Data for Discharging Flyback

I_{out} (A)	V_{out} (V)	P_{out} (W)	I_{in} (A)	V_{in} (V)	P_{in} (W)	Eff (%)
0.1	47.88	4.79	0.66	12.0	7.95	60.3
0.2	47.80	9.56	1.05	12.0	12.59	76
0.3	47.88	14.37	1.48	12.0	17.77	80.9
0.4	47.94	19.18	1.93	12.0	23.21	82.7
0.5	47.96	23.98	2.40	12.0	28.82	83.2
0.6	47.95	28.80	2.89	12.0	34.62	83.2
0.7	47.93	33.58	3.38	12.0	40.53	82.8
0.8	47.90	38.35	3.89	12.0	46.69	82.1
0.9	47.85	43.10	4.39	12.0	52.69	81.8
1.0	47.80	48.13	4.94	12.0	59.33	81.2
1.0	45.54	45.54	5.10	11.0	56.1	81.2
1.0	47.64	47.64	4.49	13.0	58.37	81.6

The average output voltage at full load is 14.56V. The drop in output voltage can be attributed to switching and copper losses. The input power and output power are calculated using the voltages and current measured from the multimeters. Efficiency of the converter was calculated using Equation 5.4.The line regulation is calculated below:

$$\text{Line Regulation} = \frac{V_{out(hi-input)} - V_{out(lo-input)}}{V_{out(nom-input)}} * 100\% = \frac{47.64V - 45.54V}{47.8V} * 100\% = 4.39\% \quad (5.6)$$

Load regulation is calculated using Equation 5.7 shown below:

$$\text{Load Regulation} = \frac{V_{out(min-load)} - V_{out(max-load)}}{V_{out(max-load)}} * 100\% = \frac{47.88V - 47.8V}{47.8V} * 100\% = 0.167\% \quad (5.7)$$

The line and load regulations of the discharging flyback are below the required 5%. Figure 5-17 shows a graph of the efficiency of the discharging stage for the bi-directional converter versus load current.

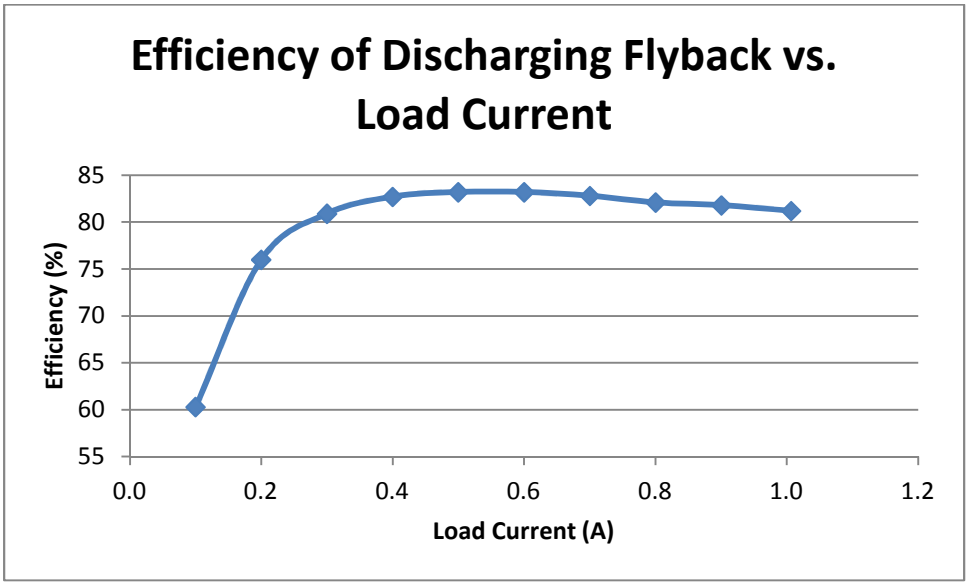

Figure 5-17: Efficiency vs. Load Current for Discharging Stage

Figure 5-18 and Figure 5-19 shows the voltage waveform at the gate pin of the discharging LT3748 IC and the drain voltage seen at the MOSFET of the discharging stage at full load conditions respectively. Figure 5-20 shows the voltage at the sense pin of the discharging LT3748 and Figure 5-21 shows the output voltage peak-to-peak ripple at full load conditions.

The output voltage peak-to-peak ripple at full load of 1A measures to be 690mV. The percentage of the output voltage that this ripple corresponds to can be calculated below:

$$\%\frac{\Delta V}{V_o} = \frac{0.690V}{47.8V} * 100\% = 1.44\% \quad (5.8)$$

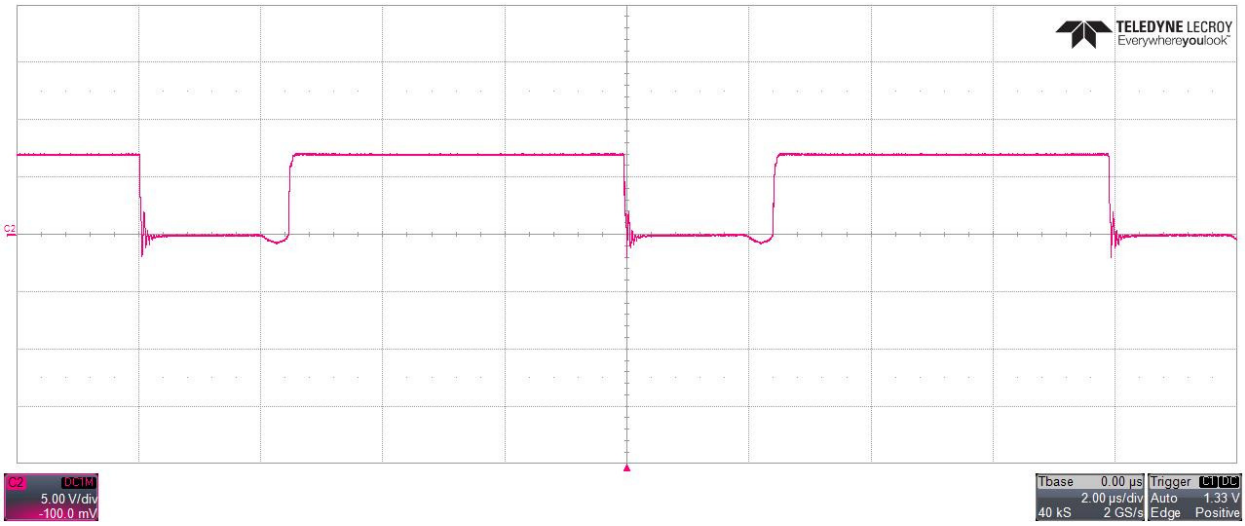

Figure 5-18: Gate Voltage of Discharging Stage LT3748

Figure 5-19: Drain-Source Voltage of Discharging Stage MOSFET

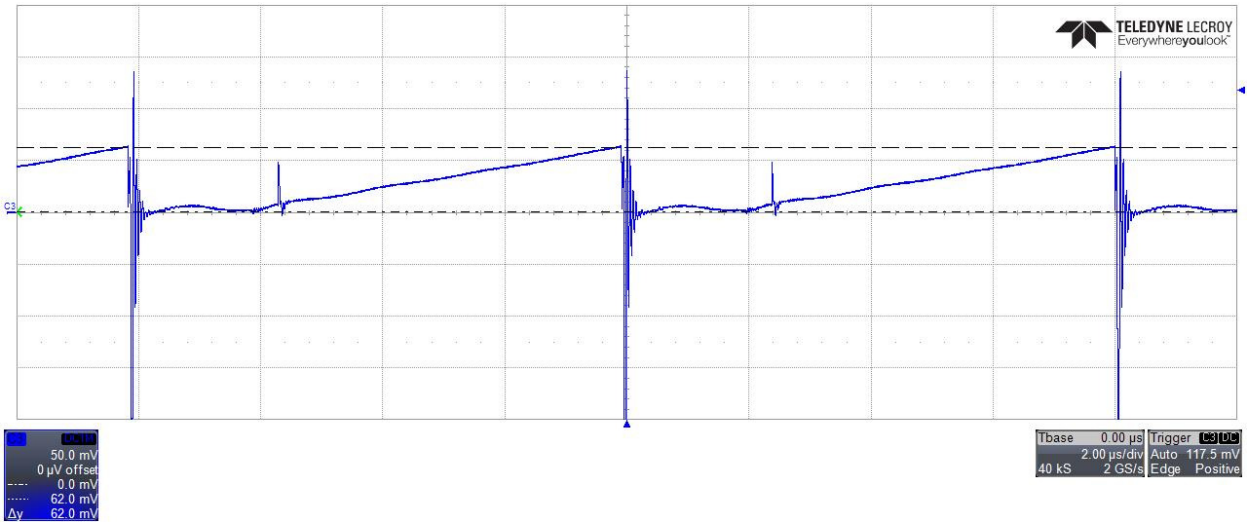

Figure 5-20: Sense pin of Discharging Stage LT3748

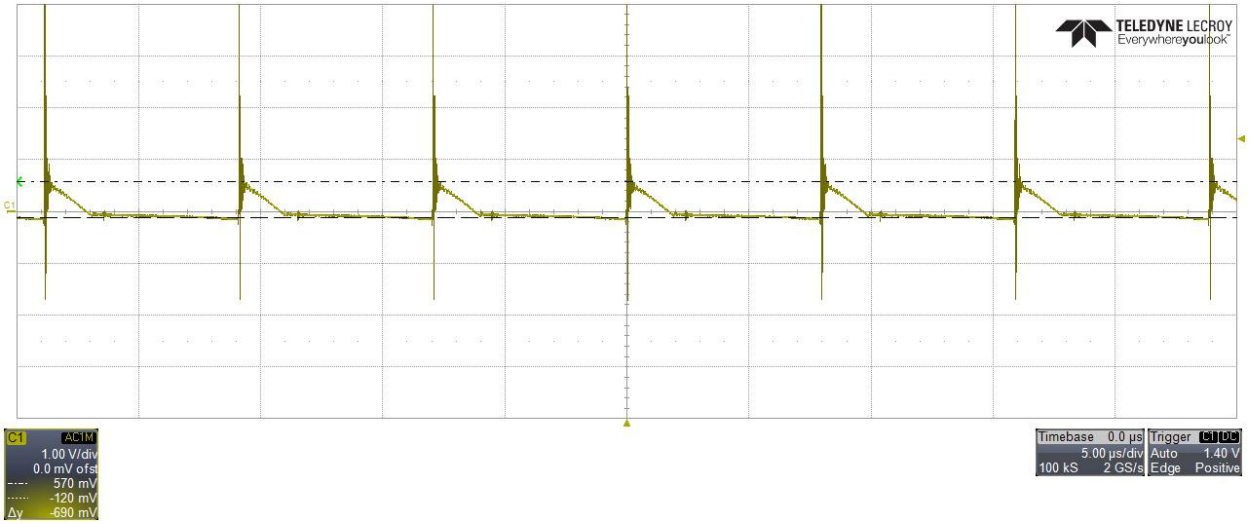

Figure 5-21: Output Voltage Peak-to-Peak Ripple of Discharging Stage

Table 5-3 summarizes the hardware results and compares them to the design requirements outlined in Chapter 3 and the simulation results from Chapter 4. All the design requirements for the bi-directional converter have been met with efficiencies above 80%, line and load regulations below 5%, and an output voltage ripple of less than 5%.

Table 5-3: Comparison Between Design, Simulation and Hardware Results

	Charging Stage			Discharging Stage		
	Design Requirement	**Simulated Results**	**Hardware Results**	**Design Requirements**	**Simulated Results**	**Hardware Results**
Input Voltage	48V	48V	48V	12V	12V	12V
Output Voltage	14V	14.375V	14.8V	48V	47.785V	47.8V
Full Load Current	2A	2A	2A	1.25A	1.25A	1A
Full Load Output Power	28W	28.75W	29.23W	60W	59.73W	48.13W
Line Regulation	5%	0.028%	0.137%	5%	0.067%	4.39%
Load Regulation	5%	0.341%	0.068%	5%	4.78%	0.167%
Output Voltage Ripple	5%	1.30%	1.46%	5%	0.44%	1.44%
Efficiency at Full Load	≥80%	93.33%	82.4%	≥80%	90.41%	81.2%

Chapter 6 – Conclusion and Future Improvements

The objective of this thesis was to improve upon the initial design of the bi-directional converter. Table 6-1 shows a comparison of the initial design results and the results of the converter discussed in this thesis.

Table 6-1: Comparison of Initial and Current Hardware Results

	Charging Stage		Discharging Stage	
	Initial Design	**Current Design**	**Initial Design**	**Current Design**
Input Voltage	48V	48V	12V	12V
Output Voltage	12V	14.8V	48.8V	47.8V
Full Load Current	2A	2A	0.7A	1A
Full Load Output Power	24W	29.23W	34W	48.13W
Line Regulation	0.25%	0.137%	1.8%	4.39%
Load Regulation	2.6%	0.068%	2.9%	0.167%
Output Voltage Ripple	16%	1.46%	8.2%	1.44%
Efficiency at Full Load	86%	82%	85%	81.2%

The initial design of the bi-directional converter provided a 12V output at 2A for the charging stage that is used to charge a lead-acid battery. However an output voltage of 12V is not enough to overcome the float voltage or natural resistance of the battery. The new design outputs 14.4V at 2A, which is enough to overcome the battery's natural resistance. The output of the discharging stage has also been improved to have a higher

power output. With the new design, there is a 44% increase in power output from 34W to 48.13W. Line and load regulations for the charging stage have also been improved and the load regulation of the discharging stage has been decreased to less than 1%. The output voltage ripple of both converters is decreased to roughly 1.5% of their respective output voltages as well.

As discussed in Chapter 4, the initial design of the control scheme had one major flaw where the battery would always be discharging even when the MISO converter that primarily supplies the DC bus line is active. The new control scheme takes into consideration the voltage level of the DC bus line to better regulate the discharging stage in hopes to further the lifespan of the lead-acid batteries and the converter will no longer discharge when the MISO is active. The new control scheme also allows the converter to operate between the voltages of 11V to 13V which correspond to a fully discharged and fully charged lead-acid battery. The initial implementation was only able to operate in the range of 11 to 11.1V [12]. The complexity of this new control scheme does however have a drawback. The overall efficiency of the converter is lower than the initial design due to additional circuitry needed to operate the bi-directional converters control.

The current output power of the discharging stage is 48W, but as outlined in Chapter 3, the desired output power is 150W. In order to increase the power output of the converter, improvements to the sensing circuitry of the LT3748 controller is required. Lowering the sense resistance may help to increase power, but will make it susceptible to high frequency noise. A more effective RC filter can be implemented to remove unwanted noise and prevent the controller from turning off incorrectly. Another path that

can be taken to improve power output would be to use different topologies like those mentioned in Chapter 2.

The efficiency of the bi-directional converter can also be improved by lowering the leakage inductances of the custom transformers. Less ringing due to the leakage will help to minimize switching losses during operation. This design also requires two transformers due to the constraints of the LT3748 controller. The inductance values that dictate the operating frequency of the converter do not fall within the same ranges for the charging and discharging stage therefore creating the need for separate transformers. The original design was able to use one transformer because of its choice in duty cycle and power output for each stage. Choosing a new controller IC for the flyback converters may allow for a single transformer.

The final implementation of this bi-directional converter will need to be incorporated with the DC House to observe the charging and discharging times of the battery needed by the house. Protection equipment such as fuses and current limiting devices on the battery side are needed to preserve the battery as well as the DC bus line that is connected directly to the DC House.

Overall, this thesis successfully met the design requirements outlined in Chapter 3 as well as made significant improvements to the initial design of the bi-directional converter that will be implemented in the DC House Project.

References

[1] U.S. Energy Information Administration. (2013). *AEO2014 Early Release Overview*.

[2] U.S. Energy Information Administration. (2013, July 25.). *EIA projects world energy consumption will increase 56% by 2040.* [Online]. Available: http://www.eia.gov/todayinenergy/detail.cfm?id=12251

[3] U.S. Energy Information Administration. (2013, July 25.). *International Energy Outlook 2013*. [Online]. Available: http://www.eia.gov/forecasts/ieo/electricity.cfm

[4] Taufik. (2011). "The DC House Project." [Online]. Available: http://www.calpoly.edu/~taufik/dchouse/index.html

[5] Taufik, (2014, Jan.). "Rural electrification: The DC House solution", The Economist, Powering Up: Perspectives on Indonesia's Energy Future.

[6] No Author. (2014). *Lead-acid battery*. [Online]. Available: http://en.wikipedia.org/wiki/Lead%E2%80%93acid_battery

[7] Progressive Dynamics, Inc. (2014). *Battery Basics*. [Online]. Available: http://www.progressivedyn.com/battery_basics.html

[8] No Author. (2013, Dec. 19.). *Battery Basics: A Layman's Guide to Batteries*. [Online]. Available: http://www.batterystuff.com/kb/articles/battery-articles/battery-basics.html

[9] No Author. (2012, Sept. 20.). *Peukert's Law | A Nerd's Attempt to Explain Battery Capacity*. [Online]. Available: http://www.batterystuff.com/kb/tools/peukert-s-law-a-nerds-attempt-to-explain-battery-capacity.html

[10] J. Zhang, "Bidirectional DC-DC Power Converter Design Optimization, Modeling and Control." Ph.D dissertation, Dept. Elect. Eng., Virginia Polytechnic Institute and State Univ., Blacksburg, VA, 2008.

[11] C.-C. Lin, L.-S. Yang, G.W. Wu, "Study of a non-isolated bidirectional DC-DC converter." Dept. of Elect. Eng., Far East University., Tainan City, Taiwan, 2012.

[12] A. Luan. "Bi-directional Flyback DC-DC Converter for Battery System of the DC House Project." M.S. Thesis, California Polytechnic State University., San Luis Obispo, California, 2013.

[13] No Author. *Charging Deep Cycle Batteries*. [Online]. Available: http://www.dynobattery.com/Charging.pdf

[14] D. Diarisso, M. Diallo, A. Diao, O. Sow, I. Gaye, F. Barro, G. Sissoko. (2013, Feb.). "Development of Battery Charge/Discharge Regulator for Photovoltaic Systems", International Journal of Innovative Technology and Exploring Engineering, Volume 2, Issue 3.

[15] S. Harrington, J. Dunlop. (1992, Aug.). "Battery Charge Controller Characteristics in Photovoltaic Systems."

[16] No Author. (2009, Nov. 6). *Basic Single-Output Flyback Converter Circuit Diagram*. [Online]. Available: http://datasheetoo.com/power-ic/switching-regulator-power-ic/basic-single-output-flyback-converter-circuit-diagram.html

[17] Linear Technology, "100V Isolated Flyback Controller," LT3748 datasheet, 2012.

[18] Taufik. Switching Mode Power Supply: Components and Design EE527 Lecture Notes. California Polytechnic State University., San Luis Obispo, California, 2014.

[19] Taufik, D. Dolan. Introduction to Power Electronics. California Polytechnic State University., San Luis Obispo, California, 2012.

[20] O. Jong. "Multiple Input Single Output (MISO) DC-DC Converter For the DC House Project." Senior Project. California Polytechnic State University., San Luis Obispo, California, 2012.

[21] No Author. *Optocouplers & Optoisolators Applications*. [Online]. Available: http://teacher.en.rmutt.ac.th/ktw/04-710-409/OPTOCOUPLER%20APPLICATIONS.htm

[22] Avago Technologies, "HCNR200 and HCNR201 High-Linearity Analog Optocouplers," HCNR200 datasheet, 2011

[23] Mag-Inc Magnetics. (2013). *Power Design*. [Online]. Available: http://www.mag-inc.com/File%20Library/Product%20Literature/Ferrite%20Literature/MagneticsFerritePowerDesign2013.pdf

[24] Mag-Inc Magnetics. (2014). *Ferrite Materials: Ferrite Cores*. [Online]. Available: http://www.mag-inc.com/products/ferrite-cores

[25] Taufik. Introduction to Magnetic Design. California Polytechnic State University. San Luis Obispo, California, 2013.

[26] Mag-Inc Magnetics. (2014). *R Material*. [Online]. Available: http://www.mag-inc.com/products/ferrite-cores/r-material

[27] Mag-Inc Magnetics. (2014). *Ferrite Pot Cores*. [Online]. Available: http://www.mag-inc.com/products/ferrite-cores/ferrite-pot-cores

[28] Ferroxcube, “PQ35/35 PQ cores and accessories,” PQ3535 datasheet, 2008.